UNIVERSITY OF CALIFORNIA SAN DIEGO

Structure and Function of Muscle in Rotator Cuff Disease

A dissertation submitted in partial satisfaction of the

requirements for the degree Doctor of Philosophy

in

Bioengineering

by

Sydnee A. Hyman

Committee in Charge:

Professor Adam J. Engler, Co-Chair
Professor Samuel R. Ward, Co-Chair
Professor Karen L. Christman
Professor Simon Schenk
Professor Sameer B. Shah
Professor Anshuman Singh

2021

The Dissertation of Sydnee A. Hyman is approved, and it is acceptable in quality and form for publication on microfilm and electronically:

_____

_____

_____

_____

_____

Co-Chair

_____

Co-Chair

University of California San Diego

2021

EPIGRAPH

When we try to pick out anything by itself, we find it hitched to everything else in the universe.

John Muir
My First Summer in the Sierra

TABLE OF CONTENTS

Signature Page....iii

Epigraph....iv

Table of Contents....v

List of Figures....viii

List of Tables....x

Acknowledgements....xi

Vita....xiii

Abstract of the Dissertation....xiv

Chapter 1. Introduction.... 1

Rotator Cuff Disease.... 1

Structure-Function Relationship in Skeletal Muscle.... 1

Structural Changes after Rotator Cuff Tear.... 2

Role of Exercise in Muscle Maintenance.... 3

References.... 5

Chapter 2. In Vivo Supraspinatus Muscle Contractility and Architecture in Rabbit.... 11

Abstract.... 11

Introduction.... 11

Materials & Methods.... 13

Results 18

Discussion 21

Acknowledgements 24

References 25

Figures 29

Chapter 3. Supraspinatus Muscle Architecture and Physiology in a Rabbit Model of Tenotomy and Repair 36

Abstract 36

Introduction 37

Materials & Methods 38

Results 43

Discussion 46

Acknowledgements 49

Figures 50

Supplemental Material 56

References 58

Chapter 4. Exercise-related Signaling Is not Impacted by Supraspinatus Tear of Repair in Rabbit 61

Abstract 61

Introduction 61

Materials and Methods 62

Results 67

Discussion 69

Acknowledgements 71

Figures 72

References 79

Chapter 5. Discussion 82

References 85

LIST OF FIGURES

Figure 2.1 Experimental setup (A) showing in vivo preparation of the scapula immobilized with the clamp attached, exposed SSP, and distal tendon attached with suture to the servomotor. 29

Figure 2.2 Intact Joint Angle-Muscle Length measurements throughout full shoulder joint flexion/extension 30

Figure 2.3 Linear regression of Activated vs. Resting muscle length 31

Figure 2.4 Average architectural values for the left (n=6 female rabbits) and right (n=5 female rabbits) side supraspinatus muscles. Raw fiber length (A) and sarcomere length (C) 32

Figure 2.5 Regional Architectural measurements for rabbit SSP.. 33

Figure 2.6 Predicted length-tension curves (dashed line) normalized to % of maximal isometric tension (P_0) for each rabbit. 34

Figure 2.7 Peak Isometric tension (A) and stress (B) for our study 35

Figure 3.1 Experimental design. Timeline for generating each experimental group 50

Figure 3.2 Architectural changes following tenotomy and repair. 51

Figure 3.3 Peak isometric force (A) and stress (B) per animal. 52

Figure 3.4 Whole muscle strain per animal (N=30, n=6 rabbits per group). 53

Figure 3.5 Predicted Length-Tension Curves for each experimental group. 54

Figure 3.6 Predicted length-tension curves (dashed line) and individual data points 55

Figure 3.7S Regional differences in normalized fiber length.. 56

Figure 4.1. Experimental design (A) showing timeline for generating experimental groups 72

Figure 4.2. Physiological comparisons. Peak isometric force (A), stress (B), and whole muscle strain (C) are shown for each experimental group. 73

Figure 4.3. Characterization of exercise bout. Average tension for each animal (A), total number of contractions for each animal (B), and the sum of the force time integral for each animal (C) are shown for each experimental group. 74

Figure 4.4 Representative immunoblots for each experimental group. 75

Figure 4.5. Fold changes in phosphorylation of JNK (A) and p38 (B) relative to pre-contraction over all groups. 76

Figure 4.6. Immunoblotting results for total JNK, pJNK, total p38, and p-p38 for all groups (N=16; n=4 control, n=6 tenotomy, n=6 repair). 77

Figure 4.7. Linear regressions of fold change in phosphorylation/total JNK (top row) and p38 (bottom row). 78

LIST OF TABLES

Table 3.1 Model parameters and values used for the predicted L-T curves 46

Table 3.2S Comparison of experimental vs. predicted curve width 56

Table 3.3S Comparison of experimental vs. predicted curve height 56

Table 3.4S Comparison of experimental vs. predicted optimal muscle length..... 57

ACKNOWLEDGEMENTS

I owe my deepest gratitude to the remarkable mentors I have worked with throughout my academic career. First, to Professors Sam Ward and Adam Engler for helping me transition research projects and forge ahead undaunted. Sam's mentorship has taught me to "plant trees, not decorate them" and the importance of scheduling priorities over prioritizing schedules. Besides pushing me as a scientist, he has helped me develop leadership skills to be the *kind* of person I want to be. I would also like to acknowledge Prof. Simon Schenk for challenging me to be clear and concise in my thinking and my language. I am also grateful to my teachers, Mr. Smoot and Ms. Mourad, for showing me how to think critically, and to Prof. Eric Nauman, for inspiring me to pursue graduate research in the first place.

Especially helpful to me have been my lab mates in the Ward lab. In particular, I would like to acknowledge Melissa Hernandez, Mackenzie Norman, Laura Vasquez-Bolanos, and Isabella Wu for their constant support and entertainment (in the cadaver lab, rabbit OR, or with our puppies). I would also like to acknowledge both Mary Esparza and Shannon Bremner, who helped troubleshoot my benchwork, let me ask them the same questions a hundred times, sectioned tissue and run assays, entertained my dancing during physiology experiments, and generously offered their years of expertise to me anytime I asked.

My success would not have been possible without the love and support of my family and friends. To my parents, Rick Hyman and Cheryl Acheson, for imparting the grit and tenacity required to drive my ambitions, and Nick Hyman, for always being my big brother. I would also like to acknowledge Julia Hardy, Ismael Munoz, Megan Jeffords, Kevin Lapp, Cole Hanson, and Christine McKee who have been the most wonderful, dedicated, and understanding friends I could ever ask for.

Finally, to my partner Anjulie Agrusa—I quite simply couldn't have done this without you.

Chapter 2, in full, is a reprint of the material as it appears in the Journal of Applied Physiology 2020. Sydnee A Hyman, Mackenzie B Norman, Shanelle N Dorn, Shannon N Bremner, Mary C Esparza, Richard L Lieber, Samuel R Ward. The dissertation author was the primary investigator of this material.

Chapter 3, in full, is currently being prepared for submission for publication of this material. Sydnee A Hyman, Isabella T Wu, Laura S Vasquez-Bolanos, Mackenzie B Norman, Shanelle N Dorn,

Shannon N Bremner, Mary C Esparza, Ivan Ramirez, Donald C Fithian, John G Lane, Anshuman Singh, Samuel R Ward. The dissertation author was the primary investigator of this material.

Chapter 4, in full, is currently being prepared for submission for publication of this material. Sydnee A Hyman, Ji Kang, Ji Park, Laura S Vasquez-Bolanos, Isabella T Wu, Mackenzie B Norman, Shanelle N Dorn, Shannon N Bremner, Mary C Esparza, Donald C. Fithian, John G. Lane, Anshuman Singh, Simon Schenk, Samuel R Ward. The dissertation author was the primary investigator of this material.

VITA

2015 Bachelor of Science, Biomedical Engineering, Purdue University

2021 Doctor of Philosophy, Bioengineering, University of California San Diego

ABSTRACT OF THE DISSERTATION

Structure and Function of Muscle in Rotator Cuff Disease

by

Sydnee A. Hyman

Doctor of Philosophy in Bioengineering

University of California, San Diego, 2021

Professor Adam Engler, Co-Chair

Professor Samuel Ward, Co-Chair

More than 30% of the population over age 60 will suffer from a rotator cuff tear. Progressive tears lead to atrophic and degenerative muscle changes that persist irrespective of therapeutic intervention, whether conservative or surgical. The degree of decreased muscle quality (retraction, atrophy, fibrosis, and fatty degeneration) serves as the strongest predictor of post-surgical functional outcomes, yet the quantitative effects on muscle physiology are poorly understood. The purpose of this work was to investigate the structural and functional implications of rotator cuff tear and repair in a rabbit model system. We first established a method to evaluate the structure-function relationship in healthy supraspinatus muscles. We then performed a detailed architectural analysis to relate the structural and physiological consequences of rotator cuff tear and repair. Finally, we evaluated the activation of mechanotransduction pathways in our model system to investigate a potential mechanism for persistent muscle loss. In summary, we characterized aspects of the altered structure-function relationship in both torn and surgically repaired rotator cuff muscles to better understand the physiological implications of disease and potential therapies.

Chapter 1. Introduction

Rotator Cuff Disease

Rotator cuff tendinopathy can cause pain, tendon degeneration, failure, and ultimately muscle retraction and atrophy, impairing shoulder function (29). These atrophic and degenerative changes associated with chronic rotator cuff (RC) tears (muscle retraction, atrophy, fibrosis, and fatty infiltration) are both difficult to treat clinically and associated with poor clinical outcomes (7, 8, 20, 25). Progressive tears are highly prevalent, impacting 30% of people over age 60 and resulting in more than 400,000 surgeries annually (8, 9, 68).

Though surgical tendon repair is common, outcomes are highly variable. Re-tear rates remain high—between 17-94%, and many patients are left with persistent functional deficits even after successful repairs (7, 28, 29). Numerous factors have been linked to postsurgical outcomes, including age, work history, tear characteristics (size and location), and muscle quality (atrophy, fibrosis, and fatty infiltration) (11, 55). More than anything else, loss of muscle quantity and quality is the strongest predictor of postsurgical shoulder function (25, 29, 35, 60).

Surprisingly, even after a clinically successful repair, muscle atrophy and fatty infiltration progression is halted, but not reversed (20, 25). Consequently, a primary focus of contemporary research is preventing muscle quality loss and/or improving muscle quality (17, 19, 37, 38, 66), but little attention has been paid to the effects of muscle quality loss on muscle function.

Structure-Function Relationship in Skeletal Muscle

Skeletal muscle has a hierarchical structure that is tightly linked with its function. Sarcomeres, the functional unit of muscle, are comprised of thin actin filaments and thick myosin filaments. The ability to generate force arises from thin and thick filament interactions, and force production is proportional to the amount of thick and thin filament overlap (27, 34). This is known as the length-tension relationship of sarcomeres, and it is central to muscle function. Sarcomeres are arranged in series to create myofilaments, which are arranged in parallel to create muscle fibers. Individual fibers are arranged in bundles, and multiple bundles come together to create whole muscles.

Skeletal muscle architecture is defined as "the arrangement of muscle fibers relative to the axis of force generation" (41) and is the primary determinant of active muscle function at the whole muscle level. The physiological cross-sectional area (PCSA) of a muscle is the best predictor of a muscle's maximum force generating capacity (4). Similarly, the normalized fiber length of a muscle (experimentally measured fiber length normalized to a ratio of optimal sarcomere length and measured sarcomere length) predicts a muscle's maximum contractile velocity (52). Taken together, the architectural characteristics of muscle can be used to predict muscle function (6, 52, 67).

Structural Changes after Rotator Cuff Tear

Given this intimate structure-function relationship in skeletal muscle, decreased muscle quality likely impairs muscle function after RC tear. However, little attention has been paid to addressing the profound architectural changes to chronically torn RC muscles (22, 62), and the physiological consequences of these muscular changes are largely unknown. One study measured supraspinatus (SSP) contractile muscle force intraoperatively in human (20), one group reported infraspinatus contractile force in sheep (18, 47), and two groups reported SSP contractile force in rabbit (13, 63) after tenotomy. Of these studies, none have measured contractile force after repair.

While decreased muscle cross sectional area (CSA) is clearly linked to decreased peak muscle force (20, 41, 47, 63), there are a number of cellular and structural changes in torn RC muscles that could also impact muscle physiology (10, 22, 23, 46). For example, a recent study in rabbit claimed that fatty infiltration was a better predictor of muscle weakness than atrophy (63). However, a variety of structural changes may impact function—shorter muscles and fiber lengths may indicate serial sarcomere loss (22, 62), which may impair muscle operating range, increased pennation angles may be a compensatory mechanism to retain some force production after tear (42, 48, 56), secondary muscle injury from repair may result in loss of excitation-contraction coupling and more fibrosis (10), further impairing force production (22, 64). Overall, further studies in muscle architecture and physiology as a function of RC tear and repair may enhance our understanding of the clinical challenges in treating RC disease.

Role of Exercise in Muscle Maintenance

The regulation of muscle maintenance is achieved through balancing both hypertrophic and atrophic pathways to enable muscles to meet their functional demands (26, 58). In healthy muscle, exercise activates hypertrophic signaling pathways, while inhibiting atrophic signaling through several axes (26, 33, 58). The primary hypertrophic response is the expression and activation of mTOR, which can be activated by IGF-1/PI3K/AKT signaling or mechanosensing (32, 50), and has many downstream actors (such as 4E-BP-1 and $p70^{s6k}$) (12, 39, 58). Mitogen activated protein kinases (MAPKs) have also been linked to the regulation of muscle hypertrophy, including c-Jun NH_2-terminal kinase (JNK) (40). Increased phosphorylation of JNK and p38 mitogen activated protein kinase (MAPK) are robust markers of muscle "activation" in response to mechanical stress, and their phosphorylation increases in a tension-dependent manner (3, 16, 40, 45, 61). Downstream effects of activation of this pathway has been linked to mRNA modulation of pro-hypertrophic genes (e.g. myostatin, mTOR, and p70s6k) (14, 31, 36, 40). Exercise has also been shown to suppress myostatin, a member of the TGFβ superfamily and negative regulator of muscle growth and myogenesis (49).

Muscle atrophy is an active process controlled by three primary proteolytic systems: calcium dependent calpains, lysosomal proteases, and the ubiquitin proteasome (MuRF1, MAFbx); all three have been implicated in RC disease (5, 58). MAFbx is primarily activated by inflammatory cytokines (TNF-α and IL-1α) via p38 activation (12, 58). Hyperplasia occurs through the activation of satellite cells for myogenesis, mediated by Pax7, MYRF4, MyoD, and myogenin expression (1, 12, 15, 21, 41, 59). Within one hour after exercise, activation of mTOR (49, 51), AKT (50, 57), $p70^{s6k}$ (50, 51), GSK-3β (57), p38 (51, 71), and NF-kB (51) have been measured by protein abundance and phosphorylation; and early gene expression has been demonstrated after loading (2, 44, 49, 53, 65, 69, 70).

Studies in RC disease have shown downregulation of hypertrophic and upregulation of atrophic, fibrotic, and adipogenic genes in humans (5, 21, 24), sheep (15, 54), and rodents (30, 43). However, it is unclear if the persistent loss in muscle quality is a result of insufficient muscle stresses and strains, or an inability of the muscle to undergo hypertrophy (7, 20, 25, 29, 60). Given the lack of hypertrophy in recovering RC disease patients, there may be a dysregulated response to exercise in diseased muscle. However, this remains untested in humans or a model system of RC disease.

References

1. Bazgir B, Fathi R, Rezazadeh Valojerdi M, Mozdziak P, Asgari A. Satellite Cells Contribution to Exercise Mediated Muscle Hypertrophy and Repair. *Cell J Yakhteh* 18: 473–484, 2017.

2. Bodine SC. mTOR signaling and the molecular adaptation to resistance exercise. *Med Sci Sports Exerc* 38: 1950–1957, 2006. doi: 10.1249/01.mss.0000233797.24035.35.

3. Boppart MD, Hirshman MF, Sakamoto K, Fielding RA, Goodyear LJ. Static stretch increases c-Jun NH2-terminal kinase activity and p38 phosphorylation in rat skeletal muscle. *Am J Physiol Cell Physiol* 280: C352-358, 2001. doi: 10.1152/ajpcell.2001.280.2.C352.

4. Burkholder TJ, Fingado B, Baron S, Lieber RL. Relationship between muscle fiber types and sizes and muscle architectural properties in the mouse hindlimb. *J Morphol* 221: 177–190, 1994. doi: 10.1002/jmor.1052210207.

5. Choo A, McCarthy M, Pichika R, Sato EJ, Lieber RL, Schenk S, Lane JG, Ward SR. Muscle Gene Expression Patterns in Human Rotator Cuff Pathology. *J Bone Joint Surg Am* 96: 1558–1565, 2014. doi: 10.2106/JBJS.M.01585.

6. Close RI. Dynamic properties of mammalian skeletal muscles. *Physiol Rev* 52: 129–197, 1972. doi: 10.1152/physrev.1972.52.1.129.

7. Collin P, Colmar M, Thomazeau H, Mansat P, Boileau P, Valenti P, Saffarini M, Nover L, Kempf JF. Clinical and MRI Outcomes 10 Years After Repair of Massive Posterosuperior Rotator Cuff Tears. *J Bone Jt Surg Am* 100: 1854–1863, 2018. doi: 10.2106/JBJS.17.01190.

8. Collin P, Thomazeau H, Walch G, Gerber C, Mansat P, Favard L, Colmar M, Kempf JF, Herve A, Betz M. Clinical and structural outcome twenty years after repair of isolated supraspinatus tendon tears. *J Shoulder Elbow Surg* 28: 196–202, 2019. doi: 10.1016/j.jse.2018.07.023.

9. Colvin AC, Egorova N, Harrison AK, Moskowitz A, Flatow EL. National Trends in Rotator Cuff Repair. *J Bone Joint Surg Am* 94: 227–233, 2012. doi: 10.2106/JBJS.J.00739.

10. Davis ME, Stafford PL, Jergenson MJ, Bedi A, Mendias CL. Muscle Fibers are Injured at the Time of Acute and Chronic Rotator Cuff Repair. *Clin Orthop* 473: 226–232, 2015. doi: 10.1007/s11999-014-3860-y.

11. Djurasovic M, Marra G, Arroyo JS, Pollock RG, Flatow EL, Bigliani LU. Revision Rotator Cuff Repair: Factors Influencing Results. *JBJS* 83: 1849–1855, 2001.

12. Egerman MA, Glass DJ. Signaling pathways controlling skeletal muscle mass. *Crit Rev Biochem Mol Biol* 49: 59–68, 2014. doi: 10.3109/10409238.2013.857291.

13. Fabis J, Kordek P, Bogucki A, Mazanowska-Gajdowicz J. Function of the rabbit supraspinatus muscle after large detachment of its tendon: 6-week, 3-month, and 6-month observation. *J Shoulder Elbow Surg* 9: 211–6, 2000.

14. Fiatarone MA, Marks EC, Ryan ND, Meredith CN, Lipsitz LA, Evans WJ. High-Intensity Strength Training in Nonagenarians: Effects on Skeletal Muscle. *JAMA* 263: 3029–3034, 1990. doi: 10.1001/jama.1990.03440220053029.

15. Frey E, Regenfelder F, Sussmann P, Zumstein M, Gerber C, Born W, Fuchs B. Adipogenic and myogenic gene expression in rotator cuff muscle of the sheep after tendon tear. *J Orthop Res* 27: 504–509, 2009. doi: 10.1002/jor.20695.

16. Fujii N, Boppart MD, Dufresne SD, Crowley PF, Jozsi AC, Sakamoto K, Yu H, Aschenbach WG, Kim S, Miyazaki H, Rui L, White MF, Hirshman MF, Goodyear LJ. Overexpression or ablation of JNK in skeletal muscle has no effect on glycogen synthase activity. *Am J Physiol-Cell Physiol* 287: C200–C208, 2004. doi: 10.1152/ajpcell.00415.2003.

17. Gerber C, Meyer DC, Nuss KM, Farshad M. Anabolic steroids reduce muscle damage caused by rotator cuff tendon release in an experimental study in rabbits. *J Bone Joint Surg Am* 93: 2189–2195, 2011. doi: 10.2106/JBJS.J.01589.

18. Gerber C, Meyer DC, Schneeberger AG, Hoppeler H, Rechenberg BV. Effect of Tendon Release and Delayed Repair on the Structure of the Muscles of the Rotator Cuff: An Experimental Study in Sheep. .

19. Gerber C, Meyer DC, Von Rechenberg B, Hoppeler H, Frigg R, Farshad M. Rotator cuff muscles lose responsiveness to anabolic steroids after tendon tear and musculotendinous retraction: an experimental study in sheep. *Am J Sports Med* 40: 2454–2461, 2012. doi: 10.1177/0363546512460646.

20. Gerber C, Schneeberger AG, Hoppeler H, Meyer DC. Correlation of atrophy and fatty infiltration on strength and integrity of rotator cuff repairs: a study in thirteen patients. *J Shoulder Elbow Surg* 16: 691–696, 2007. doi: 10.1016/j.jse.2007.02.122.

21. Gibbons MC, Fisch KM, Pichika R, Cheng T, Engler AJ, Schenk S, Lane JG, Singh A, Ward SR. Heterogeneous muscle gene expression patterns in patients with massive rotator cuff tears. *PLoS One* 13: e0190439, 2018. doi: 10.1371/journal.pone.0190439.

22. Gibbons MC, Sato EJ, Bachasson D, Cheng T, Azimi H, Schenk S, Engler AJ, Singh A, Ward SR. Muscle architectural changes after massive human rotator cuff tear. *J Orthop Res* 34: 2089–2095, 2016. doi: 10.1002/jor.23256.

23. Gibbons MC, Singh A, Anakwenze O, Cheng T, Pomerantz M, Schenk S, Engler AJ, Ward SR. Histological Evidence of Muscle Degeneration in Advanced Human Rotator Cuff Disease. *J Bone Jt Surg Am* 99: 190–199, 2017. doi: 10.2106/jbjs.16.00335.

24. Gibbons MC, Singh A, Engler AJ, Ward SR. The role of mechanobiology in progression of rotator cuff muscle atrophy and degeneration. *J Orthop Res* 36: 546–556, 2018. doi: 10.1002/jor.23662.

25. Gladstone JN, Bishop JY, Lo IKY, Flatow EL. Fatty infiltration and atrophy of the rotator cuff do not improve after rotator cuff repair and correlate with poor functional outcome. *Am J Sports Med* 35: 719–728, 2007. doi: 10.1177/0363546506297539.

26. Glass DJ. Skeletal muscle hypertrophy and atrophy signaling pathways. *Int J Biochem Cell Biol* 37: 1974–1984, 2005. doi: 10.1016/j.biocel.2005.04.018.

27. Gordon AM, Huxley AF, Julian FJ. The variation in isometric tension with sarcomere length in vertebrate muscle fibres. *J Physiol* 184: 170–192, 1966. doi: 10.1113/jphysiol.1966.sp007909.

28. Goutallier D, Postel JM, Bernageau J, Lavau L, Voisin MC. Fatty muscle degeneration in cuff ruptures. Pre- and postoperative evaluation by CT scan. *Clin Orthop* : 78–83, 1994.

29. Goutallier D, Postel J-M, Gleyze P, Leguilloux P, Van Driessche S. Influence of cuff muscle fatty degeneration on anatomic and functional outcomes after simple suture of full-thickness tears. *J Shoulder Elbow Surg* 12: 550–554, 2003. doi: 10.1016/s1058-2746(03)00211-8.

30. Gumucio JP, Davis ME, Bradley JR, Stafford PL, Schiffman CJ, Lynch EB, Claflin DR, Bedi A, Mendias CL. Rotator cuff tear reduces muscle fiber specific force production and induces macrophage accumulation and autophagy. *J Orthop Res Off Publ Orthop Res Soc* 30: 1963–1970, 2012. doi: 10.1002/jor.22168.

31. Gumucio JP, Sugg KB, Mendias CL. TGF-β superfamily signaling in muscle and tendon adaptation to resistance exercise. *Exerc Sport Sci Rev* 43: 93–99, 2015. doi: 10.1249/JES.0000000000000041.

32. Hamilton DL, Philp A, MacKenzie MG, Baar K. A limited role for PI(3,4,5)P3 regulation in controlling skeletal muscle mass in response to resistance exercise. *PloS One* 5: e11624, 2010. doi: 10.1371/journal.pone.0011624.

33. Hoppeler H, Klossner S, Flück M. Gene expression in working skeletal muscle. *Adv Exp Med Biol* 618: 245–254, 2007. doi: 10.1007/978-0-387-75434-5_19.

34. Huxley AF, Niedergerke R. Structural Changes in Muscle During Contraction: Interference Microscopy of Living Muscle Fibres. *Nature* 173: 971–973, 1954. doi: 10.1038/173971a0.

35. Kim HM, Dahiya N, Teefey SA, Keener JD, Galatz LM, Yamaguchi K. Relationship of tear size and location to fatty degeneration of the rotator cuff. *J Bone Jt Surg Am* 92: 829–39, 2010. doi: 10.2106/jbjs.H.01746.

36. Kramer HF, Goodyear LJ. Exercise, MAPK, and NF-κB signaling in skeletal muscle. *J Appl Physiol* 103: 8, 2007.

37. Lee C, Agha O, Liu M, Davies M, Bertoy L, Kim HT, Liu X, Feeley BT. Rotator Cuff Fibro-Adipogenic Progenitors Demonstrate Highest Concentration, Proliferative Capacity, and Adipogenic Potential Across Muscle Groups. .

38. Lee C, Liu M, Agha O, Kim HT, Feeley BT, Liu X. Beige FAPs Transplantation Improves Muscle Quality and Shoulder Function After Massive Rotator Cuff Tears. *J Orthop Res* 38: 1159–1166, 2020. doi: 10.1002/jor.24558.

39. Léger B, Cartoni R, Praz M, Lamon S, Dériaz O, Crettenand A, Gobelet C, Rohmer P, Konzelmann M, Luthi F, Russell AP. Akt signalling through GSK-3beta, mTOR and Foxo1 is involved in human skeletal muscle hypertrophy and atrophy. *J Physiol* 576: 923–933, 2006. doi: 10.1113/jphysiol.2006.116715.

40. Lessard SJ, MacDonald TL, Pathak P, Han MS, Coffey VG, Edge J, Rivas DA, Hirshman MF, Davis RJ, Goodyear LJ. JNK regulates muscle remodeling via myostatin/SMAD inhibition. *Nat Commun* 9: 3030, 2018. doi: 10.1038/s41467-018-05439-3.

41. Lieber R. *Skeletal muscle structure, function, and plasticity*. Wolters Kluwer Health Adis (ESP), 2011.

42. Lieber RL, Friden J. Functional and clinical significance of skeletal muscle architecture. *Muscle Nerve* : 1647–1666, 2000.

43. Liu X, Joshi SK, Samagh SP, Dang Y-X, Laron D, Lovett DH, Bodine SC, Kim HT, Feeley BT. Evaluation of Akt/mTOR activity in muscle atrophy after rotator cuff tears in a rat model. *J Orthop Res* 30: 1440–1446, 2012. doi: 10.1002/jor.22096.

44. Louis E, Raue U, Yang Y, Jemiolo B, Trappe S. Time course of proteolytic, cytokine, and myostatin gene expression after acute exercise in human skeletal muscle. *J Appl Physiol Bethesda Md 1985* 103: 1744–1751, 2007. doi: 10.1152/japplphysiol.00679.2007.

45. Martineau LC, Gardiner PF. Insight into skeletal muscle mechanotransduction: MAPK activation is quantitatively related to tension. *J Appl Physiol Bethesda Md 1985* 91: 693–702, 2001. doi: 10.1152/jappl.2001.91.2.693.

46. Mendias CL, Roche SM, Harning JA, Davis ME, Lynch EB, Sibilsky Enselman ER, Jacobson JA, Claflin DR, Calve S, Bedi A. Reduced muscle fiber force production and disrupted myofibril architecture in patients with chronic rotator cuff tears. *J Shoulder Elbow Surg* 24: 111–119, 2015. doi: 10.1016/j.jse.2014.06.037.

47. Meyer DC, Gerber C, Von Rechenberg B, Wirth SH, Farshad M. Amplitude and Strength of Muscle Contraction Are Reduced in Experimental Tears of the Rotator Cuff. *Am J Sports Med* 39: 1456–1461, 2011. doi: 10.1177/0363546510396305.

48. Meyer DC, Hoppeler H, Rechenberg B von, Gerber C. A pathomechanical concept explains muscle loss and fatty muscular changes following surgical tendon release. *J Orthop Res* 22: 1004–1007, 2004. doi: 10.1016/j.orthres.2004.02.009.

49. Peters D, Barash IA, Burdi M, Yuan PS, Mathew L, Fridén J, Lieber RL. Asynchronous functional, cellular and transcriptional changes after a bout of eccentric exercise in the rat. *J Physiol* 553: 947–957, 2003. doi: 10.1113/jphysiol.2003.048462.

50. Philp A, Hamilton DL, Baar K. Signals mediating skeletal muscle remodeling by resistance exercise: PI3-kinase independent activation of mTORC1. *J Appl Physiol Bethesda Md 1985* 110: 561–568, 2011. doi: 10.1152/japplphysiol.00941.2010.

51. Potts GK, McNally RM, Blanco R, You J-S, Hebert AS, Westphall MS, Coon JJ, Hornberger TA. A map of the phosphoproteomic alterations that occur after a bout of maximal-intensity contractions. *J Physiol* 595: 5209–5226, 2017. doi: 10.1113/JP273904.

52. Powell PL, Roy RR, Kanim P, Bello MA, Edgerton VR. Predictability of skeletal muscle tension from architectural determinations in guinea pig hindlimbs. *J Appl Physiol* 57: 1715–1721, 1984. doi: 10.1152/jappl.1984.57.6.1715.

53. Psilander N, Damsgaard R, Pilegaard H. Resistance exercise alters MRF and IGF-I mRNA content in human skeletal muscle. *J Appl Physiol* 95: 1038–1044, 2003. doi: 10.1152/japplphysiol.00903.2002.

54. Ruoss S, Möhl CB, Benn MC, von Rechenberg B, Wieser K, Meyer DC, Gerber C, Flück M. Costamere protein expression and tissue composition of rotator cuff muscle after tendon release in sheep. *J Orthop Res Off Publ Orthop Res Soc* 36: 272–281, 2018. doi: 10.1002/jor.23624.

55. Saccomanno MF, Sircana G, Cazzato G, Donati F, Randelli P, Milano G. Prognostic factors influencing the outcome of rotator cuff repair: a systematic review. *Knee Surg Sports Traumatol Arthrosc* 24: 3809–3819, 2016. doi: 10.1007/s00167-015-3700-y.

56. Sacks RD, Roy RR. Architecture of the hind limb muscles of cats: Functional significance. *J Morphol* 173: 185–195, 1982. doi: 10.1002/jmor.1051730206.

57. Sakamoto K, Arnolds DEW, Ekberg I, Thorell A, Goodyear LJ. Exercise regulates Akt and glycogen synthase kinase-3 activities in human skeletal muscle. *Biochem Biophys Res Commun* 319: 419–425, 2004. doi: 10.1016/j.bbrc.2004.05.020.

58. Sandri M. Signaling in Muscle Atrophy and Hypertrophy. *Physiology* 23: 160–170, 2008. doi: 10.1152/physiol.00041.2007.

59. Shah SA, Kormpakis I, Cavinatto L, Killian ML, Thomopoulos S, Galatz LM. Rotator cuff muscle degeneration and tear severity related to myogenic, adipogenic, and atrophy genes in human muscle. *J Orthop Res Off Publ Orthop Res Soc* 35: 2808–2814, 2017. doi: 10.1002/jor.23593.

60. Shen P-H, Lien S-B, Shen H-C, Lee C-H, Wu S-S, Lin L-C. Long-term functional outcomes after repair of rotator cuff tears correlated with atrophy of the supraspinatus muscles on magnetic resonance images. *J Shoulder Elbow Surg* 17: 1S-7S, 2008. doi: 10.1016/j.jse.2007.04.014.

61. Somwar R, Perreault M, Kapur S, Taha C, Sweeney G, Ramlal T, Kim DY, Keen J, Côté CH, Klip A, Marette A. Activation of p38 Mitogen-Activated Protein Kinase ␣ and ␤ by Insulin and Contraction in Rat Skeletal Muscle. 49: 7, 2000.

62. Tomioka T, Minagawa H, Kijima H, Yamamoto N, Abe H, Maesani M, Kikuchi K, Abe H, Shimada Y, Itoi E. Sarcomere length of torn rotator cuff muscle. *J Shoulder Elbow Surg* 18: 955–9, 2009. doi: 10.1016/j.jse.2009.03.009.

63. Valencia AP, Lai JK, Iyer SR, Mistretta KL, Spangenburg EE, Davis DL, Lovering RM, Gilotra MN. Fatty Infiltration Is a Prognostic Marker of Muscle Function After Rotator Cuff Tear. *Am J Sports Med* 46: 2161–2169, 2018. doi: 10.1177/0363546518769267.

64. Ward SR, Hentzen ER, Smallwood LH, Eastlack RK, Burns KA, Fithian DC, Friden J, Lieber RL. Rotator cuff muscle architecture: implications for glenohumeral stability. *Clin Orthop* 448: 157–63, 2006. doi: 10.1097/01.blo.0000194680.94882.d3.

65. Wilborn CD, Taylor LW, Greenwood M, Kreider RB, Willoughby DS. Effects of Different Intensities of Resistance Exercise on Regulators of Myogenesis: *J Strength Cond Res* 23: 2179–2187, 2009. doi: 10.1519/JSC.0b013e3181bab493.

66. Wilde JM, Gumucio JP, Grekin JA, Sarver DC, Noah AC, Ruehlmann DG, Davis ME, Bedi A, Mendias CL. Inhibition of p38 MAPK Signaling Reduces Fibrosis and Lipid Accumulation After Rotator Cuff Repair. *J Shoulder Elb Surg Am Shoulder Elb Surg Al* 25: 1501–1508, 2016. doi: 10.1016/j.jse.2016.01.035.

67. Winters TM, Takahashi M, Lieber RL, Ward SR. Whole muscle length-tension relationships are accurately modeled as scaled sarcomeres in rabbit hindlimb muscles. *J Biomech* 44: 109–115, 2011. doi: 10.1016/j.jbiomech.2010.08.033.

68. Yamamoto A, Takagishi K, Osawa T, Yanagawa T, Nakajima D, Shitara H, Kobayashi T. Prevalence and risk factors of a rotator cuff tear in the general population. *J Shoulder Elbow Surg* 19: 116–120, 2010. doi: 10.1016/j.jse.2009.04.006.

69. Yang Y, Creer A, Jemiolo B, Trappe S. Time course of myogenic and metabolic gene expression in response to acute exercise in human skeletal muscle. *J Appl Physiol Bethesda Md 1985* 98: 1745–1752, 2005. doi: 10.1152/japplphysiol.01185.2004.

70. Yang Y, Jemiolo B, Trappe S. Proteolytic mRNA expression in response to acute resistance exercise in human single skeletal muscle fibers. *J Appl Physiol Bethesda Md 1985* 101: 1442–1450, 2006. doi: 10.1152/japplphysiol.00438.2006.

71. Zarubin T, Han J. Activation and signaling of the p38 MAP kinase pathway. *Cell Res* 15: 11–18, 2005. doi: 10.1038/sj.cr.7290257.

Chapter 2. In Vivo Supraspinatus Muscle Contractility and Architecture in Rabbit

Abstract

The rotator cuff (RC) muscles are crucial in moving and stabilizing the glenohumeral joint, and tears can be functionally devastating. Chronic fatty and fibrotic muscle changes, which are non-responsive to surgical tendon repair, are a focus of contemporary research. The rabbit model recapitulates key biological features of human RC tears, but function and physiology are poorly characterized—limited force and stress data are inconsistent with literature norms in other mammalian species. Here, we present an improved method to assess the physiology of the rabbit SSP, and report values for healthy SSP architecture and physiology. Using female New Zealand White Rabbits (n=6) under 2% isofluorane anesthesia, the SSP was surgically isolated and maximum isometric force measured at 4-6 muscle lengths. Architectural analysis was performed, and maximum isometric stress was computed. Whole muscle length-tension curves were generated using architectural measurements to compare experimental physiology to theoretical predictions. Maximum isometric force (80.87± 5.58N) was dramatically greater than previous reports (11.06 and 16.1N, $p<0.05$). Architectural measurement of fiber length (34.25 ± 7.18mm), muscle mass (9.9 ± 0.93g), pennation angle (23.67 ± 8.32°), and PCSA (2.57 ± 0.20cm^2) were consistent with prior literature. Isometric stress (30.5 ± 3.07N/cm^2) was greater than previous reports of rabbit SSP (3.10 and 4.51 N/cm^2), but similar to mammalian skeletal muscles (15.7-30.13 N/cm^2). Previous studies underestimated peak force by ~90%, having profound implications for interpreting physiological changes as a function of disease state. Data presented here enable understanding the physiological implications of disease and repair in the RC of the rabbit.

Key Words: Rotator cuff, muscle force, muscle stress, muscle physiology, architecture

Introduction

Chronic rotator cuff (RC) tendon tears are a common source of shoulder pathology, with a 30% prevalence above age 60 (2). RC tears can cause pain, tendon degeneration, tendon failure, and ultimately muscle retraction and atrophy, impairing function (13). The long-term sequela of muscle unloading and retraction appears to be muscle atrophy and fat accumulation (8, 16, 33), which is largely non-responsive to rehabilitation (8, 39). While surgical tendon repair is common, decreased muscle quality (fibrosis, fatty infiltration, and atrophy) persists despite clinically successful repair and is correlated with poor functional outcomes (12).

Given the progressive pathophysiology of RC tears and the invasive methods needed to study them, it is difficult to study mechanisms of muscle atrophy and recovery in humans. While there has been a recent resurgence of small animal (mouse and rat) models of RC tears, the muscle phenotypes have limited severity, calling into question their utility as reasonable models of human muscle degeneration (6, 21, 25, 26). Some high quality studies have been performed in sheep which does recapitulate the persistent fatty atrophy seen in humans (8, 9). The rabbit model has emerged as an important animal model because, unlike rodent models, it recapitulates several important clinical characteristics of RC tear such as muscle retraction, muscle atrophy, fatty infiltration, and inflammation with tenotomy alone (as opposed to tenotomy and denervation required in rodent models) (5, 7, 28, 35, 41). Animal models have been used to describe tear progression in many ways (fiber size, fatty infiltration, atrophy, inflammation, etc.), and biological indicators of muscle function have been implicated in RC tears (membrane damage, fiber cytoskeletal disruption, extracellular matrix composition alteration, costamere structural disruption, altered fiber morphology, etc.) (3, 14, 36, 37, 47).

However, surprisingly little attention has been paid to the physiological consequences of RC tears. Peak force and stress production are key variables, but muscle length-tension relationships are also important to muscle function because there is architectural evidence that retracted RC muscles experience serial sarcomere loss (11). This will have significant functional implications if the remaining sarcomeres are overstretched during surgical reattachment, and the reattached muscle is subsequently forced to

operate on unusual portions of the length-tension curve (47). Despite this, few studies have measured contractile force and no studies have reported stress or the shape of the length-tension relationships for RC muscles. One study measured supraspinatus (SSP) contractile muscle force intraoperatively in human (10), one study reported infraspinatus contractile force in sheep (30), and two groups reported SSP contractile force in rabbit (4, 42). Importantly, contractile stress (calculated by dividing force by physiological cross sectional area (PCSA) (27)) in these studies was low (3.10 and 4.51 N/cm^2) (4, 42) compared to available literature of other mammalian skeletal muscle (15.7 to 30.13 N/cm^2) (1, 34, 48). Given this large discrepancy, we believe the prior studies have underestimated the rabbit SSP maximum isometric force. Based on the reported value for SSP PCSA ($2.8cm^2$) (27) and computing the average mammalian skeletal muscle specific tension from prior literature (22.8 ± 3.87 N/cm^2, n=80) (1, 34), we expected SSP isometric contractile force to be ~64N.

The primary purpose of this paper is to describe the methods required to define maximum contractile force and stress values of rabbit SSP, and secondarily to quantify the length-tension relationship of the SSP *in vivo*. This should enable researchers assessing RC tear pathology to study functional outcomes and develop novel therapies.

Materials & Methods

Surgical procedure: All experimental procedures were approved by the Institutional Animal Care and Use Committee (IACUC) of the University of California, San Diego. Six skeletally mature female New Zealand White rabbits (6 months old, mean body weight: 4.3 kg $\pm$ 0.3kg) were used to determine the length-tension relationship for the SSP. Animal preparation for contractile testing was performed as described previously (48). Briefly, rabbits were anesthetized with a subcutaneous injection of a ketamine-xylazine cocktail (50 and 5 mg/kg body mass, respectively) and maintained on 2% isoflurane anesthesia. Heart rate and oxygen saturation were monitored (VetOx, Heska Co., Fort Collins, CO) throughout the

test duration. An incision was made along the scapular spine to expose the superficial shoulder muscles. The SSP was exposed by dividing the middle trapezius and deltoid muscles to access the vertebral border of the scapula. The suprascapular nerve was isolated by blunt dissection around the anterior aspect of the SSP (29), and a cuff electrode (Pulsar 6Bp Stimulator; FHC, Bowdoinham, ME) was placed around the nerve for direct stimulation (see Fig. 1 of Winters et al. 2009 for image of electrode in use, 48). Nerve isolation was confirmed by delivering twitch stimulations and visualizing supraspinatus contraction.

Suture markers were placed at the distal and proximal muscle-tendon junctions to define muscle length in the neutral position (shoulder joint at 90°). This was chosen to recapitulate the *in vivo* configuration of the rabbit in quiet standing. Additional suture markers were placed to identify lateral, middle, and medial fascicles of the posterior aspect of the SSP (Fig. 2.1A). Sutures were used as fiducial markers to determine muscle and fascicle shortening during contraction. Intact muscle length measurements were recorded using digital calipers (Mitutoyo, accuracy of 0.01mm) at 4 joint angle positions (as determined by a goniometer): 60°, 90°, 120°, and 150°, representing the full range of glenohumeral flexion and extension. These measurements were used to correlate muscle length during contraction with the *in vivo* muscle operating range.

The distal SSP tendon was transected, released from the superior joint capsule, and sutured with two pieces of 2-0 Fiberwire (Arthrex, Naples, FL) using an infinity stitch and a modified Kessler stitch, both implemented to prevent suture slippage and tendon rupture. The suture was attached to a servomotor (Cambridge Model 310B; Aurora Scientific, Aurora, ON, Canada) and aligned with the force-generating axis of the motor. Muscle temperature was maintained at 37°C with radiant heat, heated saline, and a servo-temperature controller (Model 73A; YSI, Yellow Springs, OH). A custom-built clamp was used to immobilize the scapula, placed from the vertebral border along the scapular spine on top of the infraspinatus fossa (details below).

Scapula clamp manufacturing: The custom clamp used to stabilize the scapula was 3D printed (Creality Ender-3 Pro, Shenzhen Creality 3D Technology, Shenzhen, China) using ABS (32), with a layer height of 0.15mm, a shell thickness of 1.2mm and 30% fill. They were reamed using a drill bits (3/8" for large holes, 3/16" for medium holes, and 1/16" for small). Size 0 hex nuts were pressed into the hex indentations on the underside of the bottom piece of the clamp using a soldering iron, and then fixed into place using ABS cement (Oatey). An 0-80 screw was kept in the nut at all times to ensure that the holes didn't become obstructed. A two-inch piece of ABS rod stock (3/8" diameter) was threaded with a 5/16-18 die, leaving about ¼" unthreaded. The unthreaded end was cemented into the 3/8" hole on the bottom piece of the clamp with ABS cement and press down until flush with the underside. A one-inch piece of ABS rod stock (3/16") was also cemented into the 3/16" hole in the bottom piece of the clamp in a similar fashion, to stabilize the clamp while closed. The arm of the clamp was cemented to the top (flat) side of the top piece of the clamp, keeping the 3/8" holes aligned. When the cement was fully cured, the clamp was assembled by putting the rods from the lower piece through their respective holes on the upper piece. The two pieces were secured with a 5/16-18 wing nut. The large holes on the mounting block were tapped with 10-32 threads, and the smaller holes were tapped with 4-40 threads (Fig. 2.1B). One inch 10-32 screws were screwed through the holes on the mounting block, and the block was attached to a custom machined adapter plate using 4-40 screws. The adapter plate was attached to an XZ axis rack and pinion stage (Edmund Optics, Barrington, NJ). The XZ stage was mounted onto an adjustable angle plate (ThorLabs, Newton, NJ) set at a 30° angle to ensure the supraspinatus was contracting in a physiologically accurate direction. Three 1" partially threaded 0-80 socket head screws were used to secure the nose of the clamp and ensure sufficient scapula stabilization. During the experiment, 20 gauge needles were used to create pilot holes through the infraspinous fossa of the scapula allowing screw placement through the bone. Figure 2.1C shows a rabbit scapula with soft tissue removed and needles inserted to illustrate the orientation.

Isometric length-tension protocol: The length-tension protocol consisted of a series of 100 Hz tetanic contractions (pulse width: 0.3 ms; amplitude: 10 V) over a 640 ms period. Two-minute rest intervals were imposed between contractions to minimize fatigue. The first contraction was performed with the muscle set to its neutral length (the muscle length measured at 90° joint angle). This was chosen as the starting length to ensure that the first contraction was performed at a relatively short muscle length, likely on the ascending limb of the length-tension curve (44). For each subsequent contraction, the servomotor position was advanced 5 mm to lengthen the muscle. Resting muscle length was measured between suture markers with calipers before each contraction during the resting interval (Fig. 2.1D), to ensure suture stretch was not included in the muscle length data for the length-tension curves. This process continued until muscle force dropped significantly, indicating that the muscle was operating on the descending limb of the length-tension curve, with a minimum of four contractions per animal. Force was acquired for each contraction using a data acquisition board (610E series; National Instruments, Austin, TX) and a custom-written LabView program (National Instruments) at 4 kHz per channel. Passive tension at each muscle length was obtained by measuring the baseline force. Net peak isometric force was defined as the difference between peak active tension during the plateau region (Fig. 2.1D) and passive tension. A typical experimental muscle force trace is shown in Fig. 2.1D. Note the rapid tension rise and constant peak force clearly indicates that the muscle is contracting nearly isometrically.

Muscle and fascicle measurements: Videos of each contraction were taken at 1080p resolution and 30 fps and ImageJ software (38) was used to manually measure muscle and fascicle length in each frame. Activated muscle length was then computed from the measured muscle strain during the plateau region of each contraction (Fig. 2.1D). A representative plot of muscle length change during contraction is shown in Fig. 2.1D.

Muscle Architecture measurements: After animals were sacrificed, whole shoulders were fixed in 10% formalin in approximately the same orientation of 90° flexion to represent a neutral shoulder position. All architectural measurements were performed as previously described (11, 44). The supraspinatus was exposed by removing the superficial muscles (trapezius and deltoid), and several fascicles were marked: three regions posterior and two regions anterior (Fig. 2.1E). Muscle length and pennation angles of the marked fascicles were measured with digital calipers) before carefully removing the supraspinatus from the scapula. Muscle mass was recorded from fixed muscles, and fascicles were removed from distinct regions and measured for raw fiber length (27, 45). Subsequent sarcomere length measurements were performed using laser diffraction, as previously described (24). Individual muscle fibers were dissected from fascicles and mounted on glass slides. Sarcomere length was recorded for three individual fibers and averaged for each fascicle. Sarcomere number was calculated by dividing fiber length by sarcomere length. Physiological cross sectional area (PCSA) was calculated using the formula:

$$PCSA = \frac{mass}{\rho * L_{fn}} \cos\theta$$

where density was assumed to be 1.056g/cm^3 (45), L_{fn} is fiber length adjusted for sarcomere length, and θ is the average pennation angle for the muscle. One right side shoulder was damaged during sample preparation and discarded.

Theoretical length-tension curve: To reconcile experimental data with theoretical expectations for length-tension behavior, a length-tension curve was modeled using previously described methods (48). Briefly, a sarcomere level length-tension curve for rabbit skeletal muscle was generated: peak force was predicted at optimal sarcomere length (2.5 μm); the ascending limb started with minimum sarcomere length of 1.27 μm and the zone of single overlap beginning at 1.70 μm (67.59% maximum force); the

descending limb spanned from optimal length to maximum sarcomere length of 4.02 μm. The model was scaled from sarcomere to fiber level by multiplying sarcomere length values by serial sarcomere numbers. Then the model was scaled to the whole muscle level using architectural measurements from harvested supraspinatus muscles. This established the relationship between normalized fiber length (34.22 mm) and normalized muscle length (75.87 mm) from the average pennation angle (23.67°). The resting *in vivo* operating range for the SSP was determined using the intact muscle length-joint angle measurements, where the muscle length measured at max extension and max flexion set the lower and upper physiological limits for the muscle length range. The activated *in vivo* operating range was defined by scaling the resting muscle lengths by the average muscle strain during contraction.

Data analysis: Intact muscle length, strain, isometric tension, and isometric stress were analyzed using one-way ANOVA with *post-hoc* Tukey's test. Paired t-tests were used to compare left vs. right side architectural measurements. Two-way ANOVA with *post-hoc* Tukey's test was used to compare left vs. right differences, and Sidak's test was used to compare regional differences for architecture. Linear regression was used to analyze the resting and activated muscle lengths. A one-sample T-test was used to compare peak force and stress values to individual literature values. Significance level was set at $P < 0.05$, and data are presented as mean ± SD.

Results

Intact joint angle-muscle length: The supraspinatus muscle length shortened (76.03 to 66.30 mm) as the glenohumeral joint moved from 60°-150° in flexion/extension (Fig. 2.2)—the dominant physiological plane and range limit in the rabbit. Muscle length at 60° and 90° was significantly longer ($p < 0.05$) than at 150° (full flexion). This length range represented the resting *in vivo* operating range for the muscle.

Muscle and fascicle strain: Strain for the whole muscle and three fascicles was measured during each contraction (from the resting length to the activated length during the plateau region of each contraction). A strong linear correlation ($r^2 = 0.93$) was observed between resting pre-contraction length and the activated length (Fig. 2.3A). Average muscle, lateral fascicle, mid fascicle, and medial fascicle strains were measured over all contractions (6.8%, 20.95%, 20.7%, 21.31%). Strains among fascicles were not significantly different (Fig. 2.3B) and were overall larger than whole muscle strain ($p < 0.05$). This is consistent with the behavior of a pennate muscle where small muscle strain corresponds to large fascicle strain.

Muscle architecture: Paired t-tests were used to compare the left and right sides, with a total of 5 pairs of shoulders used, since one right side was lost during sample preparation. No significant differences were found between the left (experimental) and right (control) sides for normalized fiber length, sarcomere number, muscle mass, pennation angle, or PCSA (Fig. 2.4). Raw fiber length and sarcomere lengths between left and right were significantly different ($p = 0.0453$, $p = 0.0005$, respectively), which was expected since the supraspinatus had been tenotomized immediately prior to physiology testing, causing mechanical unloading and subsequent muscle retraction.

Regionally, differences between left and right sides were the result of the transection of the tendon for performing the experiment (Fig. 2.5): the pennation angle was greater and raw fiber length nearest the myotendinous junction (P1) were shortened, and all sarcomere lengths except the A2 region were significantly shortened due to muscle recoil. Between regions, fiber lengths are significantly larger from lateral to medial (P1 vs P3 and A1 vs A2), while sarcomere lengths are not different. Pennation angles are smaller from lateral to medial as the longer fibers align more closely with the force generating

axis of the muscle. Statistical significance was determined from *post hoc* Tukey's or Sidak's tests with $p < 0.05$.

Theoretical length-tension curve: Experimental whole muscle length-tension curves are typically shaped as inverted parabolas (Fig. 2.6). Resting muscle length (Fig. 2.6A) is shifted right compared to activated muscle length (Fig. 2.6B) because the muscle shortens during contraction (22, 23, 40, 49). Activated muscle length is computed from the real-time muscle strain measurements during contraction. The *in vivo* operating range (shown as the solid line on both plots) encompasses the shallow ascending limb for the resting length (Fig. 2.6A) but includes both ascending limbs for the activated length (Fig. 2.6B). This corresponds to a contractile force variation of ~30% at the resting muscle length and ~40% at the activated muscle length.

Maximum isometric force and stress: Experimentally measured maximum isometric force SSP production (80.87 ± 5.58N) (Fig. 2.7A) was significantly greater compared to prior reports (11.06 ± 1.62N and 16.1 ± 1.7N, $p<0.05$) (4, 43). Maximum stress (30.5 ± 3.07N/cm^2) (Fig. 2.7B) was, therefore, significantly greater than SSP stress values we calculated from the previously reported force measurements (3.01 and 4.51 N/cm^2, $p<0.05$) (4, 43). However, measured stress was within the range of other mammalian skeletal muscles (range 15.7 to 30.13 N/cm^2) (1, 34).

Discussion

The purpose of this study was to determine the maximum contractile force and stress and, secondarily to understand the normal length-tension behavior for the rabbit SSP. We predicted the peak isometric tension using methods and architecture previously described (27, 48) to benchmark our experimental expectations. We measured maximum isometric force, which was significantly higher than previously described (4, 42). After performing a detailed architectural assessment of the SSP, we generated a theoretical length-tension curve to attempt to explain our experimental data based on classic muscle physiology (1). Using intact resting muscle length values and whole muscle contraction strain, we determined the *in vivo* operating range of the SSP. The activated muscle length-tension curve was computed by scaling resting muscle length by the strain decrease measured during contraction and is shifted left compared to the resting muscle length-tension curve, as it incorporates muscle shortening with tendon elongation during contraction.

This is the first study to calculate the stress in rabbit SSP during maximal isometric contraction. Our predictions were based on the specific tension of mammalian skeletal muscle, 22.8N/cm^2 (1, 34), since this was previously shown to correlate strongly with PCSA in rabbit hindlimb muscles (48). Although our stress value (30.5 ± 3.07N/cm^2) was slightly higher than expected, it fell within the range reported in the literature (15.7 to 30.13N/cm^2).

Architecturally, we report similar pennation angle and muscle lengths to prior studies, but longer fiber lengths and larger muscle mass (27). Consequently, PCSA values were lower in our study compared to prior literature. The increased muscle mass and animal size could explain the longer fiber lengths in our study, but these scaling relationships are not well understood. Architecturally the gross anatomy and substructure is similar to the human SSP, as the regions of the muscle were subdivided according to prior work in human SSP architecture (44).

The predicted length-tension curve was fairly consistent with the resting muscle lengths, which are the typical muscle length measurements used (42, 48); but was improved when using the activated muscle length, as the curve shifts to the left (Fig. 2.6). The rabbit SSP is highly pennate, contains a robust internal tendon, and has heterogeneous fiber lengths; all three factors of which complicate whole muscle modeling (15, 17, 20, 23, 31). However, the primary function of the model in this case was to determine the testing range for muscle lengths and provide a reasonable estimate of maximum contractile force, making it sufficient for the scope of this study.

The leftward shift for the activated muscle lengths is largely explained by the series compliance in the muscle-tendon unit and muscle strain during contraction (22, 23, 40, 49). While the muscle-tendon unit maintains a fixed length, the muscle shortens and tendon lengthens (22, 49). This is crucially important, as the resting muscle length cannot reliably be used to estimate contractile force generation in a muscle-tendon unit with a long and/or compliant tendon (46). If resting muscle length is used to predict optimal muscle length in this system, when the muscle strains early during contraction, the muscle will shorten against the lengthening tendon. As a result, the active tension measured with a resting muscle starting length would be a sub-maximal contraction (Fig. 2.1D). This is illustrated clearly over the ascending limbs of the length-tension curve: as the muscle shortens, force decreases. Given the average whole muscle strain of 6.8% during contraction, corresponding to a discrepancy in predicted force production of ~30-40%.

The force generation we report is significantly higher than previously described (4, 42). There are several potential contributing factors to this discrepancy: Primarily, in previous studies, tetanic tension was recorded only at the muscle length that yielded the greatest twitch tension. However, due to the significant muscle strain during contraction, this would yield a sub-maximal tetanic tension because of the high series compliance in this system and the relatively brief “active state” of the twitch itself (18). Additionally, firmly fixing both ends of the system (the scapula and the released tendon) is challenging, and any movement in the system decreases the recorded force due to the drop in force that occurs as the

muscle shortens (19). This leads to why the resting muscle length is insufficient to measure maximal tension since the relationship between resting length and optimal length varies based on muscle and connective tissue anatomy in a muscle-specific and species-specific manner (1, 20, 22, 23, 40, 46). This is also the reason that we generated the entire length-tension curve so as not to assume the relationship between the two parameters for this muscle. Finally, isolating and reliably stimulating the suprascapular nerve can also prove challenging. The current study used female NZW rabbits with a mean body weight of 4.3 kg, whereas the previous studies used slightly smaller rabbits (Fabis et al. used 3-4 kg "mixed race" males and Valencia et al. used 2.3 kg NZW and did not indicate gender). Despite these differences, to our knowledge there are no difference in contractility based on gender for 6 month old rabbits, and no available published data regarding the growth curve for body weight vs. SSP size. However, even if body weight and SSP size scale linearly, a 50% difference in body mass would correlate with a 50% difference in supraspinatus mass. With a 50% smaller muscle we would expect roughly 50% lower force production, not the much greater 90% difference that we observed.

This study has several limitations. First, interference from the infraspinatus (ISP), which is also innervated by the suprascapular nerve could theoretically increase our force recordings. We aimed to isolate the SSP by releasing the tendon lateral to medial (approximately 1 cm) from the ISP tendon, but we did not surgically separate the muscle bellies of SSP and ISP. However, the scapular spine serves as a bony separation between SSP and ISP muscles, making direct force transmission from the ISP unlikely. Additionally, stress values are similar to the vast majority of other mammalian skeletal muscle reports (1, 34, 48). Taken together, we believe our values represent the SSP and not interference by the ISP. Because we believe we have completely separated the distal tendons, and lateral force transmission is negligible because of the scapular spine, if release differences were contributing to measured force differences among the various studies, then other studies would have been reporting higher, not lower forces. However, if we test the muscles at a short resting length, we get similar results to the other studies. This is why testing at multiple muscle lengths (especially longer lengths) is important to ensure the maximum

isometric forces are captured. This is uniquely important in the rabbit SSP system because significant shortening strains are observed in the muscle-tendon unit, even when the bones are adequately secured. Second, we assume that our maximum recorded force is on the plateau of the length-tension curve for each rabbit, which could produce a shift the curve. Third, we did not measure real-time changes in sarcomere length during contractions, and thus we can only make indirect correlations to the physiologic operating range of the SSP through intact muscle length-joint angle relationships and measured muscle strain during contraction. Lastly, the modeling strategy we employed was developed for hindlimb muscles, not highly pennate muscles with high series elasticity, potentially influencing the accuracy of the model.

In summary, this study describes the methods to isolate the rabbit supraspinatus, immobilize the scapula, and perform physiology testing to assess its length-tension relationship. We report the maximum contractile force generation for the muscle and a detailed architectural analysis, allowing for computation of muscle stress. These methods will be useful for future investigations into the physiological effects of rotator cuff tear and subsequent repair in animal systems, which is clinically valuable (9, 10, 16, 43).

Acknowledgements

This chapter, in full, is a reprint of the material as it appears in the Journal of Applied Physiology, 2020. Sydnee A Hyman, Mackenzie B Norman, Shanelle N Dorn, Shannon N Bremner, Mary C Esparza, Richard L Lieber, Samuel R Ward. The dissertation author was the primary investigator of this material.

References

1. Close RI. Dynamic properties of mammalian skeletal muscles. *Physiol Rev* 52: 129–197, 1972. doi: 10.1152/physrev.1972.52.1.129.

2. Collin P, Thomazeau H, Walch G, Gerber C, Mansat P, Favard L, Colmar M, Kempf JF, Herve A, Betz M. Clinical and structural outcome twenty years after repair of isolated supraspinatus tendon tears. *J Shoulder Elbow Surg* 28: 196–202, 2019. doi: 10.1016/j.jse.2018.07.023.

3. Davis ME, Stafford PL, Jergenson MJ, Bedi A, Mendias CL. Muscle Fibers are Injured at the Time of Acute and Chronic Rotator Cuff Repair. *Clin Orthop* 473: 226–232, 2015. doi: 10.1007/s11999-014-3860-y.

4. Fabis J, Kordek P, Bogucki A, Mazanowska-Gajdowicz J. Function of the rabbit supraspinatus muscle after large detachment of its tendon: 6-week, 3-month, and 6-month observation. *J Shoulder Elbow Surg* 9: 211–6, 2000.

5. Farshad M, Meyer DC, Nuss KMR, Gerber C. A modified rabbit model for rotator cuff tendon tears: functional, histological and radiological characteristics of the supraspinatus muscle. *Shoulder Elb* 4: 90–94, 2012. doi: 10.1111/j.1758-5740.2011.00170.x.

6. Farshad M, Würgler-Hauri CC, Kohler T, Gerber C, Rothenfluh DA. Effect of age on fatty infiltration of supraspinatus muscle after experimental tendon release in rats. *BMC Res Notes* 4: 530, 2011. doi: 10.1186/1756-0500-4-530.

7. Gerber C, Meyer DC, Nuss KM, Farshad M. Anabolic steroids reduce muscle damage caused by rotator cuff tendon release in an experimental study in rabbits. *J Bone Joint Surg Am* 93: 2189–2195, 2011. doi: 10.2106/JBJS.J.01589.

8. Gerber C, Meyer DC, Schneeberger AG, Hoppeler H, Rechenberg BV. Effect of Tendon Release and Delayed Repair on the Structure of the Muscles of the Rotator Cuff: An Experimental Study in Sheep. .

9. Gerber C, Schneeberger AG, Beck M, Schlegel U. Mechanical strength of repairs of the rotator cuff. *J Bone Jt Surg Br* 76: 371–80, 1994.

10. Gerber C, Schneeberger AG, Hoppeler H, Meyer DC. Correlation of atrophy and fatty infiltration on strength and integrity of rotator cuff repairs: a study in thirteen patients. *J Shoulder Elbow Surg* 16: 691–696, 2007. doi: 10.1016/j.jse.2007.02.122.

11. Gibbons MC, Sato EJ, Bachasson D, Cheng T, Azimi H, Schenk S, Engler AJ, Singh A, Ward SR. Muscle architectural changes after massive human rotator cuff tear. *J Orthop Res* 34: 2089–2095, 2016. doi: 10.1002/jor.23256.

12. Gladstone JN, Bishop JY, Lo IKY, Flatow EL. Fatty infiltration and atrophy of the rotator cuff do not improve after rotator cuff repair and correlate with poor functional outcome. *Am J Sports Med* 35: 719–728, 2007. doi: 10.1177/0363546506297539.

13. Goutallier D, Postel J-M, Gleyze P, Leguilloux P, Van Driessche S. Influence of cuff muscle fatty degeneration on anatomic and functional outcomes after simple suture of full-thickness tears. *J Shoulder Elbow Surg* 12: 550–554, 2003. doi: 10.1016/s1058-2746(03)00211-8.

14. Gumucio JP, Davis ME, Bradley JR, Stafford PL, Schiffman CJ, Lynch EB, Claflin DR, Bedi A, Mendias CL. Rotator cuff tear reduces muscle fiber specific force production and induces macrophage accumulation and autophagy. *J Orthop Res Off Publ Orthop Res Soc* 30: 1963–1970, 2012. doi: 10.1002/jor.22168.

15. Herring SW, Grimm AF, Grimm BR. Functional heterogeneity in a multipinnate muscle. *Am J Anat* 154: 563–575, 1979. doi: 10.1002/aja.1001540410.

16. Hersche O, Gerber C. Passive tension in the supraspinatus musculotendinous unit after long-standing rupture of its tendon: A preliminary report. *J Shoulder Elbow Surg* 7: 393–396, 1998. doi: 10.1016/S1058-2746(98)90030-1.

17. Herzog W, ter Keurs HEDJ. Force-length relation of in-vivo human rectus femoris muscles. *Pflüg Arch* 411: 642–647, 1988. doi: 10.1007/BF00580860.

18. Hill AV. The mechanics of active muscle. *Proc R Soc Lond Ser B - Biol Sci* 141: 104–117, 1953. doi: 10.1098/rspb.1953.0027.

19. Hill AV. The effect of load on the heat of shortening of muscle. *Proc R Soc Lond B Biol Sci* 159: 297–318, 1964. doi: 10.1098/rspb.1964.0004.

20. Kawakami Y, Lieber RL. Interaction between series compliance and sarcomere kinetics determines internal sarcomere shortening during fixed-end contraction. *J Biomech* 33: 1249–1255, 2000. doi: 10.1016/s0021-9290(00)00095-6.

21. Kim HM, Galatz LM, Lim C, Havlioglu N, Thomopoulos S. The effect of tear size and nerve injury on rotator cuff muscle fatty degeneration in a rodent animal model. *J Shoulder Elbow Surg* 21: 847–858, 2012. doi: 10.1016/j.jse.2011.05.004.

22. Lieber RL, Brown CG, Trestik CL. Model of muscle-tendon interaction during frog semitendinosis fixed-end contractions. *J Biomech* 25: 421–428, 1992. doi: 10.1016/0021-9290(92)90261-X.

23. Lieber RL, Leonard ME, Brown CG, Trestik CL. Frog semitendinosis tendon load-strain and stress-strain properties during passive loading. *Am J Physiol-Cell Physiol* 261: C86–C92, 1991. doi: 10.1152/ajpcell.1991.261.1.C86.

24. Lieber RL, Yeh Y, Baskin RJ. Sarcomere length determination using laser diffraction. Effect of beam and fiber diameter. *Biophys J* 45: 1007–1016, 1984.

25. Liu X, Laron D, Natsuhara K, Manzano G, Kim HT, Feeley BT. A mouse model of massive rotator cuff tears. *J Bone Joint Surg Am* 94: e41, 2012. doi: 10.2106/JBJS.K.00620.

26. Liu X, Manzano G, Kim HT, Feeley BT. A rat model of massive rotator cuff tears. *J Orthop Res Off Publ Orthop Res Soc* 29: 588–595, 2011. doi: 10.1002/jor.21266.

27. Mathewson MA, Kwan A, Eng CM, Lieber RL, Ward SR. Comparison of rotator cuff muscle architecture between humans and other selected vertebrate species. *J Exp Biol* 217: 261–273, 2014. doi: 10.1242/jeb.083923.

28. Matsumoto F, Uhthoff HK, Trudel G, Loehr JF. Delayed tendon reattachment does not reverse atrophy and fat accumulation of the supraspinatus--an experimental study in rabbits. *J Orthop Res Off Publ Orthop Res Soc* 20: 357–363, 2002. doi: 10.1016/S0736-0266(01)00093-6.

29. McCracken TO, Kainer RA, Carlson D. Color Atlas of Small Animal Anatomy: The Essentials, Revised Edition [Online]. Wiley-Blackwell. https://www.wiley.com/en-us/Color+Atlas+of+Small+Animal+Anatomy%3A+The+Essentials%2C+Revised+Edition-p-9780813816081 [24 Aug. 2020].

30. Meyer DC, Gerber C, Von Rechenberg B, Wirth SH, Farshad M. Amplitude and Strength of Muscle Contraction Are Reduced in Experimental Tears of the Rotator Cuff. *Am J Sports Med* 39: 1456–1461, 2011. doi: 10.1177/0363546510396305.

31. Morgan DL. From sarcomeres to whole muscles. *J Exp Biol* 115: 69–78, 1985.

32. Muscle Physiology Lab. Rabbit Scapula Clamp [Online]. UC San Diego. http://muscle.ucsd.edu/projects/downloads.shtml.

33. Petersen SA, Murphy TP. The timing of rotator cuff repair for the restoration of function. *J Shoulder Elbow Surg* 20: 62–68, 2011. doi: 10.1016/j.jse.2010.04.045.

34. Powell PL, Roy RR, Kanim P, Bello MA, Edgerton VR. Predictability of skeletal muscle tension from architectural determinations in guinea pig hindlimbs. *J Appl Physiol* 57: 1715–1721, 1984. doi: 10.1152/jappl.1984.57.6.1715.

35. Rubino LJ, Stills HF, Sprott DC, Crosby LA. Fatty infiltration of the torn rotator cuff worsens over time in a rabbit model. *Arthrosc J Arthrosc Relat Surg Off Publ Arthrosc Assoc N Am Int Arthrosc Assoc* 23: 717–722, 2007. doi: 10.1016/j.arthro.2007.01.023.

36. Ruoss S, Möhl CB, Benn MC, von Rechenberg B, Wieser K, Meyer DC, Gerber C, Flück M. Costamere protein expression and tissue composition of rotator cuff muscle after tendon release in sheep. *J Orthop Res Off Publ Orthop Res Soc* 36: 272–281, 2018. doi: 10.1002/jor.23624.

37. Sato EJ, Killian ML, Choi AJ, Lin E, Esparza MC, Galatz LM, Thomopoulos S, Ward SR. Skeletal muscle fibrosis and stiffness increase after rotator cuff tendon injury and neuromuscular compromise in a rat model. *J Orthop Res Off Publ Orthop Res Soc* 32: 1111–1116, 2014. doi: 10.1002/jor.22646.

38. Schindelin J, Arganda-Carreras I, Frise E, Kaynig V, Longair M, Pietzsch T, Preibisch S, Rueden C, Saalfeld S, Schmid B, Tinevez J-Y, White DJ, Hartenstein V, Eliceiri K, Tomancak P, Cardona A. Fiji: an open-source platform for biological-image analysis. *Nat Methods* 9: 676–682, 2012. doi: 10.1038/nmeth.2019.

39. Shen P-H, Lien S-B, Shen H-C, Lee C-H, Wu S-S, Lin L-C. Long-term functional outcomes after repair of rotator cuff tears correlated with atrophy of the supraspinatus muscles on magnetic resonance images. *J Shoulder Elbow Surg* 17: 1S-7S, 2008. doi: 10.1016/j.jse.2007.04.014.

40. Trestik CL, Lieber RL. Relationship between Achilles tendon mechanical properties and gastrocnemius muscle function. *J Biomech Eng* 115: 225–230, 1993. doi: 10.1115/1.2895479.

41. Uhthoff HK, Matsumoto F, Trudel G, Himori K. Early reattachment does not reverse atrophy and fat accumulation of the supraspinatus--an experimental study in rabbits. *J Orthop Res Off Publ Orthop Res Soc* 21: 386–392, 2003. doi: 10.1016/S0736-0266(02)00208-5.

42. Valencia AP, Iyer SR, Pratt SJP, Gilotra MN, Lovering RM. A method to test contractility of the supraspinatus muscle in mouse, rat, and rabbit. *J Appl Physiol 1985* 120: 310–7, 2016. doi: 10.1152/japplphysiol.00788.2015.

43. Valencia AP, Lai JK, Iyer SR, Mistretta KL, Spangenburg EE, Davis DL, Lovering RM, Gilotra MN. Fatty Infiltration Is a Prognostic Marker of Muscle Function After Rotator Cuff Tear. *Am J Sports Med* 46: 2161–2169, 2018. doi: 10.1177/0363546518769267.

44. Ward SR, Hentzen ER, Smallwood LH, Eastlack RK, Burns KA, Fithian DC, Friden J, Lieber RL. Rotator cuff muscle architecture: implications for glenohumeral stability. *Clin Orthop* 448: 157–63, 2006. doi: 10.1097/01.blo.0000194680.94882.d3.

45. Ward SR, Lieber RL. Density and hydration of fresh and fixed human skeletal muscle. *J Biomech* 38: 2317–2320, 2005. doi: 10.1016/j.jbiomech.2004.10.001.

46. Ward SR, Loren GJ, Lundberg S, Lieber RL. High Stiffness of Human Digital Flexor Tendons Is Suited for Precise Finger Positional Control. *J Neurophysiol* 96: 2815–2818, 2006. doi: 10.1152/jn.00284.2006.

47. Ward SR, Sarver JJ, Eng CM, Kwan A, Würgler-Hauri CC, Perry SM, Williams GR, Soslowsky LJ, Lieber RL. Plasticity of Muscle Architecture After Acute Supraspinatus Tear. *J Orthop Sports Phys Ther* 40: 729–735, 2010. doi: 10.2519/jospt.2010.3279.

48. Winters TM, Takahashi M, Lieber RL, Ward SR. Whole muscle length-tension relationships are accurately modeled as scaled sarcomeres in rabbit hindlimb muscles. *J Biomech* 44: 109–115, 2011. doi: 10.1016/j.jbiomech.2010.08.033.

49. Zajac FE. Muscle and tendon: properties, models, scaling, and application to biomechanics and motor control. *Crit Rev Biomed Eng* 17: 359–411, 1989.

Figures

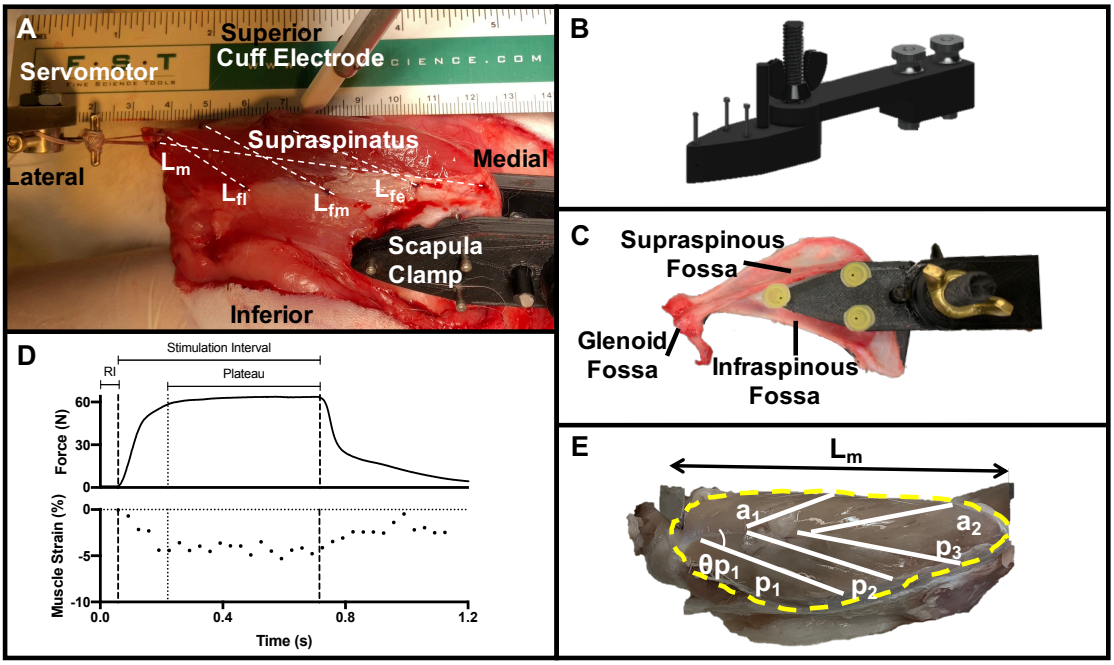

Figure 2.1 Experimental setup (A) showing *in vivo* preparation of the scapula immobilized with the clamp attached, exposed SSP, and distal tendon attached with suture to the servomotor. Care was taken to ensure proper alignment of the tendon with axis of the motor. The cuff electrode is attached to the suprascapular nerve on the superior anterior aspect of the SSP. Dotted lines connect the suture markers indicating muscle length (L_m), lateral fascicle length (L_{fl}), mid fascicle length (L_{fm}), and medial fascicle length (L_{fe}). CAD image of custom made scapula clamp (B) illustrating the components required for assembly. Isolated scapula with clamp attached (C) to illustrate the position of scapula and clamp for experimentation. Representative traces (D) of force, and muscle strain during the nerve stimulation interval. The resting interval (RI) prior to contraction indicates when the resting muscle length is measured, and the plateau indicates where the peak isometric force and muscle strain are measured. Superior-inferior view of formalin fixed SSP muscle, indicating the regions used for architectural analysis (E).

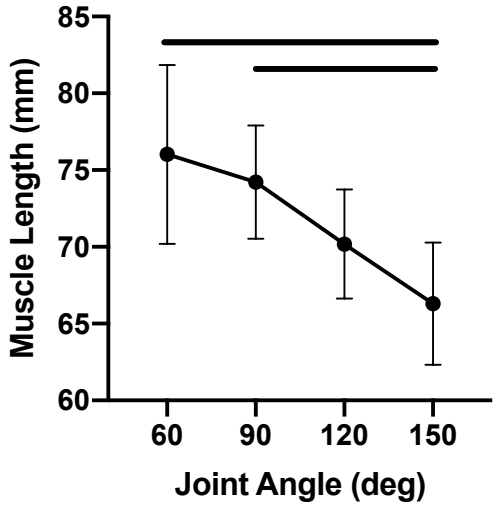

Figure 2.2 Intact Joint Angle-Muscle Length measurements throughout full shoulder joint flexion/extension (n=6 female rabbits)). Muscle length was significantly shorter from 60° and 90° to 150° ($p < 0.05$ analyzed with ANOVA with *post hoc* Tukey's test). Significance shown with horizontal lines. Points represent mean ± SD.

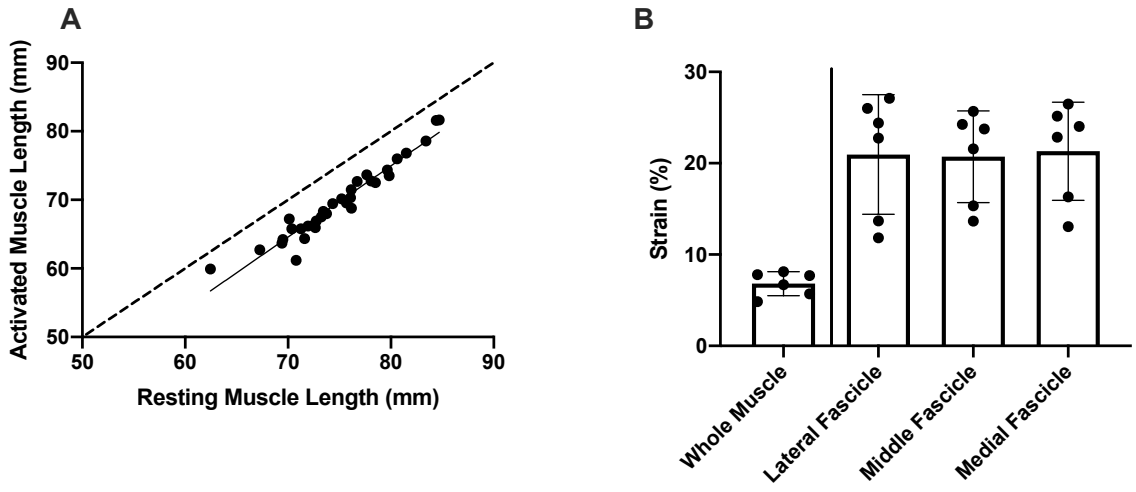

Figure 2.3 Linear regression of Activated vs. Resting muscle length (A) ($R^2 = 0.93$) with a line of identity (dashed), and each point representing one contraction (n = 31 contractions from 6 female rabbits). Average strains during contraction (B) for all contractions (n = 31 from 6 female rabbits) show that strains between fascicles are not significantly different, and fascicle strains are larger than whole muscle strain ($p < 0.05$, one-way ANOVA with *post hoc* Tukey's test). Bars represent mean ± SD.

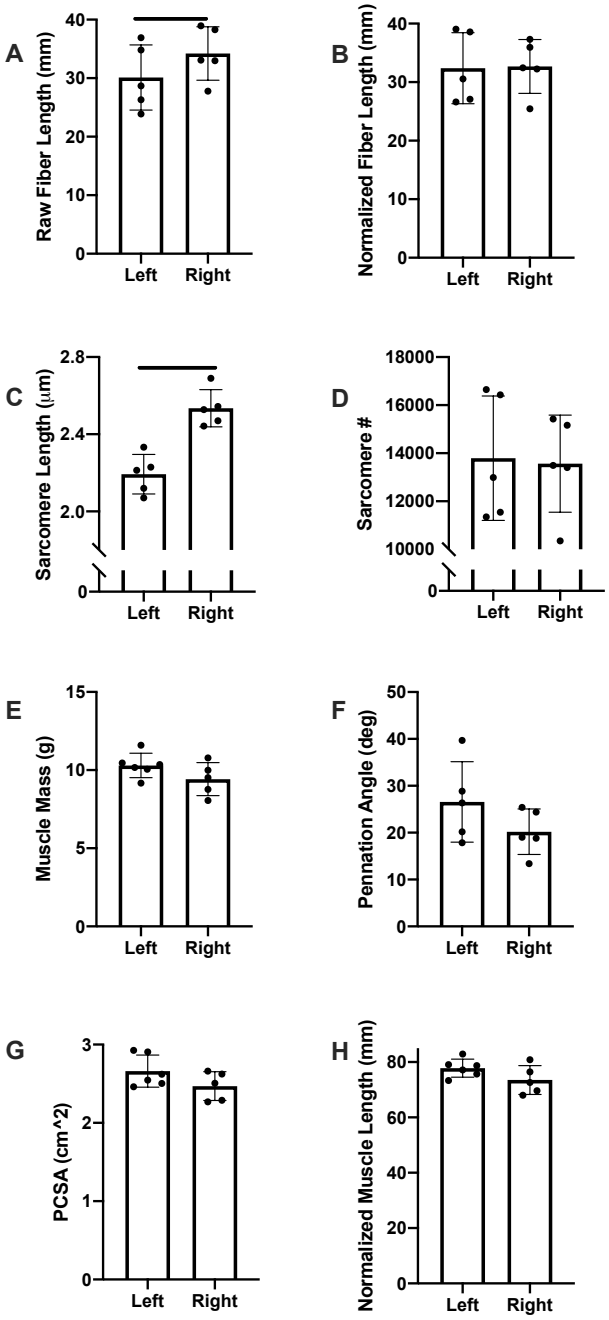

Figure 2.4 Average architectural values for the left (n=6 female rabbits) and right (n=5 female rabbits) side supraspinatus muscles. Raw fiber length (A) and sarcomere length (C) were significantly shorter on the left side ($p = 0.0453$, $p = 0.0005$). Normalized fiber length (B), sarcomere number, muscle mass, pennation angle, PCSA, and normalized muscle length (D-H) were similar between left and right sides. Analyzed with Paired t-test. Bars represent mean ± SD.

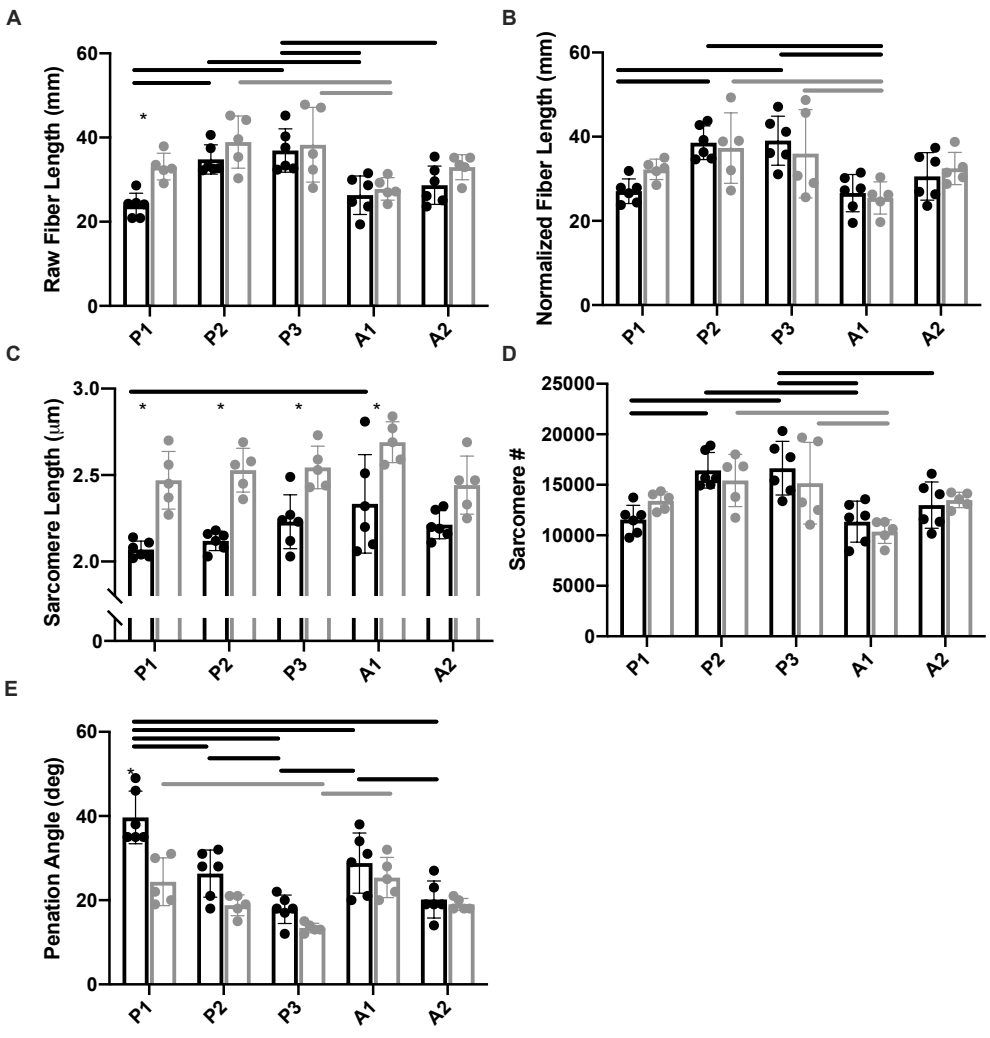

Figure 2.5 Regional Architectural measurements for rabbit SSP. Left (black, n=6 female rabbits) and right (gray, n=5 female rabbits) sides are shown for each muscle region (P1, P2, P3, A1, and A2). Two-way ANOVA with *post hoc* Tukey's test and Sidak's test was used to analyze left vs right side and regional differences, respectively. Lines represent inter-region differences (black lines for left side and gray lines for right side), and asterisks represent intra-region differences between left and right side. Raw fiber length (A), Normalized fiber length (B), and Sarcomere number (D), all show increases in the medial regions (P3 and A2) compared to the lateral regions (P1 and A1). The left side P1 region raw fiber length (A) was significantly shorter than right side, but after normalization (B) is not different. Sarcomere lengths were significantly different between sides in the P1, P2, P3, and A1 regions. Pennation angle (E) was significantly greater on left P1 region compared to right, and decreased moving from lateral to medial. These data are consistent with what is expected after the muscle is released at its tendinous insertion to the greater tubercle. Bars represent mean ± SD. *$p < 0.05$.

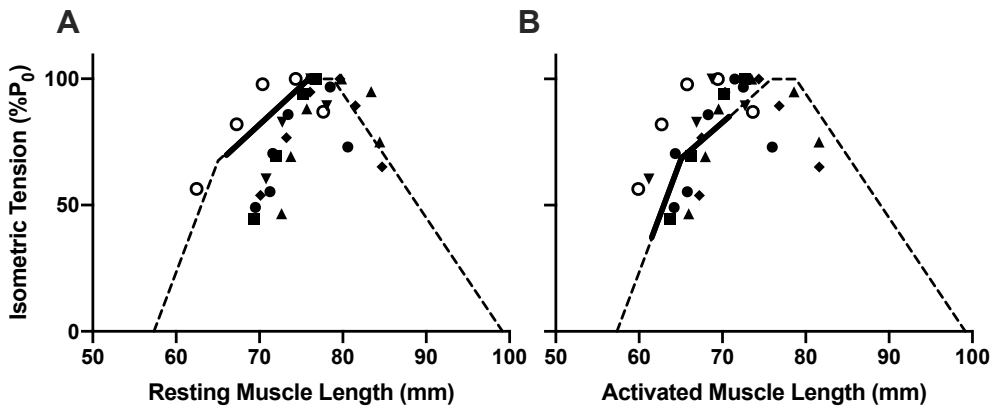

Figure 2.6 Predicted length-tension curves (dashed line) normalized to % of maximal isometric tension (P_0) for each rabbit. *In vivo* operating range shown as solid line. Resting muscle lengths were experimentally measured prior to each muscle contraction (A), while activated muscle lengths were computed using the measured muscle strain during the contraction plateau (B). The leftward shift of the activated muscle lengths highlights the importance of measuring the muscle length during contraction (activated) as opposed to prior to contraction (resting). Each point represents one contraction (n = 31), with different symbols used for each animal (n = 6 female rabbits).

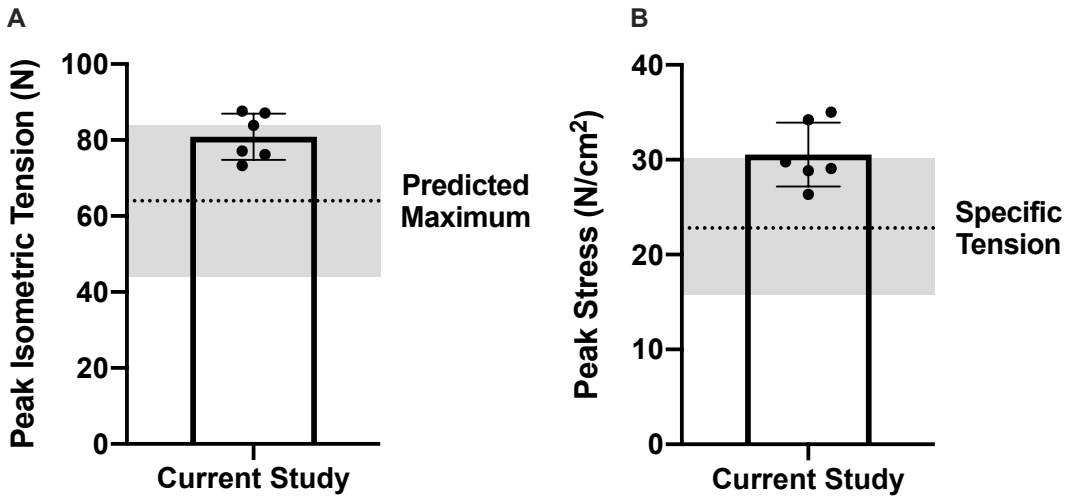

Figure 2.7 Peak Isometric tension (A) and stress (B) for our study (n=6 female rabbits). Bars represent mean ± SD. Gray bands represent the range of prior studies for muscle stress and corresponding predicted muscle force in mammalian skeletal muscle.

Chapter 3. Supraspinatus Muscle Architecture and Physiology in a Rabbit Model of Tenotomy and Repair

Abstract

Chronic rotator cuff tendon tears can cause severe functional deficits. Addressing the reversal of chronic fatty and fibrotic muscle changes is of high clinical interest; however, the architectural and physiological consequences of chronic tear and repair are poorly characterized. Here, we present a detailed architectural and physiological analysis of chronic tear (over 8 and 16 weeks) and repair (over 8 and 16 weeks) compared to age-matched control rabbit supraspinatus (SSP) muscles. Using female New Zealand White Rabbits (N=30, n=6/group) under 2% isofluorane anesthesia, the SSP was surgically isolated and maximum isometric force measured at 4-6 muscle lengths. Architectural analysis was performed, and maximum isometric stress was computed. Whole muscle length-tension curves were generated using architectural measurements to compare experimental physiology to theoretical predictions. Architectural measures are consistent with persistent radial and longitudinal atrophy over time in tenotomy that fail to fully recover after surgical repair. Maximum isometric force was significantly decreased after 16 wks of tenotomy and not significantly improved after repair. Values for peak isometric force are greater than prior reports of rabbit SSP force production after tenotomy. Peak stress values were not significantly different between groups and consistent with prior literature of SSP stress. Muscle strain during contraction was significantly decreased after 8 wks of tenotomy and repair, indicating profound effects of tear and repair on muscle function. The experimental length-tension data was overlaid with predicted curves for each experimental group (generated from structural data), highlighting the altered structure-function relationship for tenotomy and repair over time. Data presented here enable understanding the physiological implications of disease and repair in the RC of the rabbit.

Introduction

Chronic rotator cuff (RC) tendon tears cause progressively decreased muscle quality (atrophy, fatty infiltration, and fibrosis) that persists despite clinically successful repair (1, 13). These changes to the muscles are not only painful and functionally devastating to the patient, but are also predictive of negative surgical outcomes (7, 12, 15, 26, 30). While the focus of some contemporary research has been on halting or reversing the fibrosis, fatty infiltration, and atrophy (5, 6, 36), little attention has been paid to addressing the profound architectural changes to chronically torn RC muscles (10, 31). Both decreased muscle quality and changes in muscle architecture are likely to effect muscle function, yet the physiological consequences of these muscular changes after RC tear and repair are largely unknown. One study measured supraspinatus (SSP) contractile muscle force intraoperatively in human (9), one group reported infraspinatus contractile force in sheep (7, 24), and two groups reported SSP contractile force in rabbit (3, 33) after tenotomy. Of these studies, none have measured contractile force after repair.

While decreased muscle cross sectional area (CSA) has a clear link to decreased peak muscle force (9, 17, 24, 33), there are a number of cellular and structural changes in torn RC muscles that could impact muscle physiology (2, 10, 11, 23). For example, a recent study in rabbit claimed that fatty infiltration was a better predictor of muscle weakness than atrophy (33). However, a variety of structural changes may impact function - shorter muscles and fiber lengths may indicate serial sarcomere loss (10, 31), which may impair muscle operating range, increased pennation angles may be a compensatory mechanism to retain some force production after tear (18, 25, 28), secondary muscle injury from repair may result in loss of E-C coupling and more fibrosis (2), further impairing force production (10, 34). However, no in-depth evaluation of the architectural changes that occur after tear and repair have been performed in an animal model.

Therefore, the objective of this study is to measure the architectural changes and physiological consequences of rotator cuff tenotomy and repair. To reasonably recapitulate several important clinical characteristics of RC tear (muscle retraction, muscle atrophy, fatty infiltration, and inflammation), we

used a rabbit model (4, 6, 21, 27, 32). We hypothesize that architectural features will demonstrate radial and longitudinal atrophy, tenotomy and repair will cause more strain during contraction, and muscle function will be impaired (measured by peak isometric force and narrow length-tension curves). This should enable researchers assessing RC tear pathology to benchmark functional outcomes and test the functional consequences of novel therapies.

Materials & Methods

Animals: All experimental procedures were approved by the Institutional Animal Care and Use Committee (IACUC) of the University of California, San Diego. Thirty Skeletally mature female New Zealand White Rabbits (n=6/group) were used for this study. The animals used for intervention groups (both 8 and 16 wk tenotomy, and 8 and 16 wk repair) were 6 months old at the beginning of the study. To account for animal growth over the course of the study, control rabbits were age-matched to the final age of the intervention group rabbits, roughly 1 year old (Fig. 3.1A). Mean body weight at sacrifice was 4.36kg, 4.05kg, 4.30kg, 4.57kg, 4.24kg for the age-matched control, 8 wk tenotomy, 16 wk tenotomy, 8 wk repair, and 16 wk repair groups, respectively.

Cage locations were assigned upon arrival, each rabbit was given a number ID, and then randomized to one of the study groups. Researchers were aware of the allocation during the surgeries and tissue harvest, but the specimens were identified by ID number only. Animals were single-housed with food and water ad lib, environmental and food enrichment, and visual access to other animals. There were no adverse events in this study and no animals met the criteria for humane endpoints. These criteria included: displaying clinical signs of disease, loss of appetite, weight below 15% of what is expected for the animal, and/or signs of distress, such as self-mutilation.

Surgical Procedures: For all surgical procedures, rabbits were anesthetized with a subcutaneous injection of a ketamine-xylazine cocktail (50 and 5 mg/kg body mass, respectively) and maintained on 2% isoflurane anesthesia. Heart rate and oxygen saturation were monitored (VetOx, Heska Co., Fort Collins, CO) throughout the test duration. The left supraspinatus (SSP) muscle served as the experimental side in all animals, with the contralateral shoulder as an unoperated internal control.

All intervention groups underwent the following tenotomy procedure. An open anterior approach was performed on the left shoulder, followed by sharp transection of the left SSP tendon from its footprint on the greater tuberosity of the humerus. The surrounding soft tissues were bluntly dissected to allow unhindered retraction of the tendon stump and distal muscle. After securing a Penrose drain to the tendon stump to prevent scar formation between the tendon and surrounding soft tissue, the incision was closed in layers.

Rabbits were then allowed individual cage activity with routine post-operative care. Buprenorphine SR (0.1mg/kg) was used for analgesia, and the animals were monitored daily for 2 weeks post-operatively.

The two repair groups underwent a SSP repair procedure 8 weeks after tenotomy. Using the same anesthesia and anterior approach as the tenotomy, the repair was performed using a modified locking suture with anterior and posterior bone tunnels to restore the tendon footprint to the humeral head. Fibrous adhesions and any remaining tendon stump on the greater tubercle of the humerus was scraped away to allow for tendon-to-bone healing after SSP repair. Closure and post-operative protocols were the same as above.

All animals underwent the following procedure to test the length-tension relationship in the SSP using methods previously described (16). Briefly, under anesthesia, an open approach was used to expose the SSP by dividing the middle trapezius and deltoid muscles. The suprascapular nerve was isolated by blunt dissection around the anterior aspect of the SSP (22), and a cuff electrode (Pulsar 6Bp Stimulator;

FHC, Bowdoinham, ME) was placed around the nerve for direct stimulation. Nerve isolation was confirmed by delivering twitch stimulations and visualizing supraspinatus contraction. The distal SSP tendon was transected, released from the superior joint capsule, sutured to a servomotor (Cambridge Model 310B; Aurora Scientific, Aurora, ON, Canada), and aligned with the force-generating axis of the motor (Fig. 3.1B, C, and D for representative images of control, tenotomy, and repair animals in the experimental configuration). Muscle temperature was maintained at 37°C with radiant heat, heated saline, and a servo-temperature controller (Model 73A; YSI, Yellow Springs, OH). A custom-built clamp was used to immobilize the scapula, placed from the vertebral border along the scapular spine on top of the infraspinatus fossa.

Isometric length-tension protocol: The length-tension protocol was performed as previously described (16). Briefly, a series of 100 Hz tetanic contractions (pulse width: 0.3 ms; amplitude: 10 V) over a 640 ms period were delivered every two minutes. The first contraction was performed with the muscle set to its neutral length (the muscle length measured at 90° joint angle). For each subsequent contraction, the servomotor position was advanced 5 mm to lengthen the muscle. This was repeated until the muscle was operating on the descending limb of the length-tension curve, with a minimum of four contractions per animal.

Muscle and fascicle measurements: Suture markers were placed to define muscle and fascicle length, as done previously (16). Videos of each contraction were taken at 1080p resolution and 30 fps and ImageJ software (29) was used to manually measure muscle and fascicle length in each frame. Activated muscle length was then computed from the measured muscle strain during the plateau region of each contraction.

Muscle Architecture measurements: After animals were sacrificed, whole shoulders were fixed in 10% formalin in approximately the same orientation of 90° flexion to represent a neutral shoulder position. All architectural measurements were performed as previously described (10, 16, 34). The supraspinatus was exposed by removing the superficial muscles (trapezius and deltoid), and several fascicles were marked: three regions posterior and two regions anterior. Muscle length and pennation angles of the marked fascicles were measured with digital calipers before carefully removing the supraspinatus from the scapula. Muscle mass was recorded from fixed muscles, and fascicles were removed from distinct regions and measured for raw fiber length (20, 35). Subsequent sarcomere length measurements were performed using laser diffraction, as previously described (19). Individual muscle fibers were dissected from fascicles and mounted on glass slides. Sarcomere length was recorded for three individual fibers and averaged for each fascicle. Sarcomere number was calculated by dividing fiber length by sarcomere length. Physiological cross sectional area (PCSA) was calculated using the formula:

$$PCSA = \frac{mass}{\rho * L_{fn}} \cos\theta$$

where density was assumed to be 1.056g/cm^3 (35), L_{fn} is fiber length adjusted for sarcomere length, and θ is the average pennation angle for the muscle. Values averaged over all regions of the muscle are reported here, and individual regional data is included in the supplemental material (Fig. 3.1S). One pair of shoulders for the 8 wk repair group was damaged during sample preparation and discarded.

Theoretical length-tension curve: To incorporate the structural data with anticipated physiological effects, a length-tension curve was modeled for each experimental group using previously described methods (37). Briefly, a sarcomere level length-tension curve for rabbit skeletal muscle was generated: peak force was predicted at optimal sarcomere length (2.5 μm); the ascending limb started with minimum sarcomere length of 1.27 μm and the zone of single overlap beginning at 1.70 μm (67.59% maximum force); the descending limb spanned from optimal length to maximum sarcomere length of 4.02 μm. The model was scaled from sarcomere to fiber level by multiplying sarcomere length values by serial sarcomere numbers. Then the model was scaled to the whole muscle level using architectural measurements from harvested supraspinatus muscles (Table 1). The following relationship was derived for determining the predicted muscle lengths:

$$L_m = L_{mn} + \left[L_f \sqrt{1 - \left(\frac{L_{fn} \sin \theta_n}{L_f} \right)^2} - \left[L_{fn} \cos(\theta_n) \right] \right]$$

where L_m is muscle length, L_{mn} is optimal muscle length, L_f is fiber length, L_{fn} is optimal fiber length (determined from measured sarcomere length and raw fiber length), θ_n is the average pennation angle. The resting *in vivo* operating range for the SSP was determined using the intact muscle length-joint angle measurements, where the muscle length measured at max extension and max flexion set the lower and upper physiological limits for the muscle length range. The activated *in vivo* operating range was defined by scaling the resting muscle lengths by the average muscle strain during contraction.

Data analysis: Two-way ANOVA was used to compare architectural differences. *Post-hoc* Sidak's test was used to compare groups, and Fischer's LSD test was used to compare experimental vs. contralateral side differences. Muscle strain, isometric tension, and isometric stress were analyzed using one-way ANOVA to compare the main effect of intervention and with *post-hoc* Tukey's test for between group comparisons. Two-way ANOVA with *post-hoc* Sidak's tests were used to compare full width at half maximum (FWHM), peak force, and optimal muscle length between experimental and predicted length-tension curves and intervention groups. Significance level was set at $P < 0.05$ for all tests, and data are presented as mean ± SD.

Results

Muscle Architectural Changes: Supraspinatus muscle mass was significantly decreased in every intervention group (8 and 16 wk tenotomy, and 8 and 16 wk repair) compared to the unoperated side ($p=0.0043$, $p<0.0001$, $p=0.0017$, and $p=0.0005$, respectively). Both the 8 and 16 wk tenotomy groups had significantly decreased muscle mass compared with control animals, while neither of the repair groups were significantly lower than controls (Fig 3.2A). Raw muscle length was significantly shorter after both 8 and 16 wk tenotomy, and 8 wk repair (Fig 3.2B), increasing slightly from 9% shorter in the 8 wk tenotomy group to 4% shorter at 8 weeks after repair. However, no differences were noted with respect to age-matched controls. Raw fiber length decreased across all intervention groups in comparison to the contralateral side and age-matched controls (Fig 3.2C), except the 8 wk tenotomy group showed no difference from age-matched controls. However, the 8 wk tenotomy group had significantly longer fibers than 8 wk repair ($p=0.0256$).

Mean sarcomere length significantly increased to 2.40 μm at 8 weeks after repair, compared to 2.14 μm (age-matched controls) and 2.18 (16 wk repair), as well as compared with 2.20 μm on the contralateral side ($p=0.0076$, $p=0.0211$, and $p=0.0054$, respectively) (Fig 3.2D). At the same timepoint,

mean sarcomere number was 9864, significantly lower than both age-matched controls (12219), 8 wk tenotomy (11788), and its contralateral side (12156) ($p=0.0119$, $p=0.013$, and $p<0.0001$ respectively) (Fig 3.2E). After 16 weeks of tenotomy, serial sarcomere number decreased compared with its contralateral side, despite sarcomere length remaining unchanged, indicative of serial sarcomere deletion (Fig 3.2D and E). The normalized fiber length remained shorter than the contralateral side only for the 8 wk repair group ($p=0.0003$), and it was also significantly shorter than both age-matched controls and 8 wk tenotomy ($p=0.0119$ and $p=0.0131$, respectively) (Fig 3.2F).

Pennation angle showed the most differences between experimental conditions. All intervention groups showed significantly higher angles than the contralateral side (Fig 3.2G), with the largest mean pennation angle of 36.56 ° at 8 wk post-repair compared to 22.23 in control animals, a difference of 40%. Only the 8 wk tenotomy group did not show a significant increase compared to age-matched controls. Both 8 and 16 wk tenotomy had a significantly lower mean pennation angle than 8 wk repair, but there was no difference in angles between 8 and 16 wk repair.

Finally, the calculated physiological cross-sectional area was 29% lower at 8 weeks after tenotomy compared to age-matched controls ($p=0.0056$). Both 8 and 16 wk tenotomy, and 16 wk repair had a lower PCSA than the contralateral side ($p=0.0005$, $=<0.0001$, and $p=0.0085$, respectively) (Fig 3.2H).

Peak Isometric Force and Stress: Peak isometric force was significantly decreased ($p < 0.05$) after 16 wk tenotomy, compared to the control group (Fig. 3.3A). While not statistically significant, peak isometric force decreased by 22.4% after 8 wk tenotomy (Fig. 3.3A). After 8 wk repair, force 10% increased over 16 wk tenotomy, but is still 25.13% lower than the control. Peak force production not different between repair groups (67.00N and 69.70 N, 8 and 16 wk repair, respectively). 8 wk tenotomy is

very similar to both 8 wk and 16 wk repair (69.46 vs. 67.00 and 69.70 N, respectively). Peak stress is not significantly different between groups (Fig. 3.3B).

Muscle strain: The whole muscle strain during contraction was averaged for each animal (Fig. 3.4). Interestingly, both the 8 wk tenotomy and 8 wk repair groups showed the lowest mean muscle strain (4.06 and 4.54%, respectively). Compared to the control animals (7.86% strain), significant differences were noted between 8 wk tenotomy, and 8 and 16 wk repair. Muscle strain was significantly increased between 8 and 16 wk tenotomy, and 8 wk tenotomy compared to 16 wk repair. 8 wk repair was significantly lower than control, 16 wk tenotomy, and 16 wk repair.

Predicted L-T Curves: The predicted curves (Fig 3.5) were generated for each group from the architecture data from each group (Table 3.1). After 8 wk tenotomy, the curve is shifted left to shorter muscle lengths, the curve is wider because of the increased pennation angle (despite shorter fibers), and peak tension is lower because of the PCSA. After 16 wk tenotomy, the curve is narrower and taller than 8 wk tenotomy, but still has a lower predicted peak than control. After 8 wk repair, the curve is similar in width and position to 8 wk tenotomy, with increased peak tension due to PCSA increase. Comparing 16 wk repair to 8 wk repair, the curve is shifted right due to increased muscle length, narrower due to decrease in pennation angle, and peak is similar due to unchanged PCSA. The predicted curve for 16 wk repair is most similar to the control curve. The predicted curves were statistically compared using three parameters: curve width (described by Full Width at Half Max (FWHM)), curve height (described by Peak Isometric Force), and the length of peak force (described by Optimal Muscle Length) with a one-way ANOVA and post-hoc Tukey's test. No significant differences were measured.

Table 3.1 Model parameters and values used for the predicted L-T curves

	Control	8 wk Ten	16 wk Ten	8 wk Rep	16 wk Rep
Muscle Length (mm)	80.71	74.79	77.27	75.78	79.45
Sarcomere Number (#)	12219	11788	10814	9864	10721
Pennation Angle (deg)	22.23	28.73	29.4	36.56	30.2
PCSA (cm^2)	3.86	2.77	3.09	3.6	3.46

Experimental Physiology: Experimental whole muscle length-tension curves were approximated as inverted parabolas (Fig. 3.6). Activated muscle length was computed from the real-time muscle strain measurements during contraction, as was previously shown to better describe the length-tension behavior of the SSP than resting muscle length (16). The control and 8 wk tenotomy animals (Fig. 3.6A and B) most closely match the ascending limb and plateau of the predicted curve. 16 wk tenotomy (Fig. 3.6C) is shifted left from the predicted curve. 8 wk repair (Fig. 6D) was the most disordered group studied. 16 wk repair (Fig. 3.6E) is shifted right compared to the predicted curve, but the peak force is aligned with the prediction.

As above, the experimental and predicted curves were statistically compared using three parameters: curve width (described by FWHM), curve height (described by Peak Isometric Force), and the length of peak force (described by Optimal Muscle Length) with a one-way ANOVA and post-hoc Sidak's test. FWHM (Table 3.1S) was significantly different between the experimental and predicted curves for each group except for 8 wk repair ($p = 0.4125$). There were no significant differences between experimental and predicted curve height (Table 3.2S) or optimal muscle length (Table 3.3S) for any group.

Discussion

The purpose of this study was to determine the structural and physiological consequences of rotator cuff tear and surgical repair over time through measuring muscle architecture and the length-tension relationship. Our hypotheses that architectural changes would demonstrate radial and longitudinal atrophy after tear and persist through repair, and that peak force would be decreased after tenotomy and repair, were supported. Muscle strain was lower after 8 wk tenotomy and repair, and similar to normal at 16 wk tenotomy and repair, refuting our hypothesis. Our hypothesis that length-tension curves would be narrower after tenotomy and repair was supported only after 16 wk repair, and it seemed that the length-tension curves varied for each intervention group in different ways.

The architectural consequences of tenotomy indicate that muscle retraction and prolonged mechanical unloading lead to serial sarcomere loss, consistent with prior literature (11, 31). Despite the shorter fibers, the increased pennation angle seemed to overall maintain the width of the length-tension curve, which is consistent with Gerber et al.'s hypothesis that pennation angle increase is a compensatory mechanism to increase the force output and muscle excursion in the shortened, atrophied muscle (25). By 16 weeks after tenotomy (Fig. 3.2), there is significant muscle loss, indicating sarcomere loss both in parallel (by muscle mass and PCSA decrease), and in series (by sarcomere number decrease).

After repair, sarcomere lengths are dramatically lengthened at 8 weeks, indicating that the serial sarcomere loss persists in the initial stage after repair. The increased pennation angle at 8 weeks suggests a lengthening of the tendon (as opposed to muscle), in order to reattach the muscle-tendon unit to the footprint. By 16 weeks, some muscle mass and length are covered, as well as sarcomere number and sarcomere length, indicating some functional recovery of the muscle.

Whole muscle strain is vastly different between experimental groups. After 8 weeks of tenotomy, muscle strain is decreased by nearly 50%, which is not explained by structural changes (sarcomere length and sarcomere # are unchanged after 8 wk tenotomy compared to the contralateral side or control animals, Fig. 3.2). However, fibrosis is known to inhibit muscle strain, and could be largely responsible for this

decrease (14, 23). This appears to be similar after 8 weeks of repair, which has been shown to induce an acute muscle injury itself, increasing muscle fibrosis (23). However, it is unlikely that this fibrosis predominates the physiological changes 8 weeks post repair. After 16 weeks of either tenotomy or repair, muscle strain increases closer to the control animals. Many biological changes occurring to the muscle (fibrosis, muscle degeneration, fatty infiltration, etc.) which are not explored here, may be competing to influence muscle function (4, 21, 27).

Peak isometric tension was only significantly lowered after 16 weeks of tenotomy and stress was not significantly different between any groups. However, we believe these are likely under-powered results, as there are large percentage changes (~20-30%) between groups. A *post-hoc* power analysis shows an n=12 is required to detect statistical differences between these experimental groups. These data are consistent with our prior study in normal rabbits (16), but higher than previously reported by other groups in rabbit (3, 33). Despite larger animal masses used here, we believe the primary difference is due to the determination of optimal muscle length through twitch tensions, rather than maximal tetanic contractions at multiple muscle lengths. This is due to the muscle shortening during contraction, leading the optimal muscle length to be longer at rest than the twitch tensions would suggest. Peak muscle stress in this study is slightly lower than our previous study in normal rabbit SSP, but within the range of normal literature.

The physiological consequences of tear and repair are seen in the experimental length-tension curves. The control animals are tightly clustered along the ascending limb and plateau of the length-tension curves. However, all of the intervention groups differ from their predicted curves in different ways (Fig. 3.6). Curve height is highly variable for 8 wk tenotomy, 16 wk tenotomy, and 8 wk repair, but less variable in 16 wk repair. Optimal muscle length is fairly well predicted in 8 wk tenotomy, but not 16 wk tenotomy or 8 wk repair. Curve width also matches the predicted curve for 8 wk tenotomy, but not the other three intervention groups. This could be due to the varying levels of fiber shortening, muscle fibrosis (therefore stiffening), and fatty degeneration that are occurring in the muscles (11, 18, 37).

Ultimately, the numerous changes occurring to the muscle after tenotomy (atrophy, degeneration, fibrosis, fatty infiltration, etc.) are dynamic processes which occur simultaneously, and they all contribute to physiological performance. From this study, we show that measures of PCSA are able to predict peak muscle force fairly well, which has high clinical value for estimating muscle function (8, 9, 15, 33).

This study has several limitations. First, the high experimental variability in groups and relatively low sample sizes make statistical comparisons difficult, and the study would benefit from greater sample size. Second, we assume that our maximum recorded force is on the plateau of the length-tension curve for each rabbit, which could produce a shift in the curve. Third, our model utilizes averages across the entire muscle, rather than incorporating regional heterogeneity into account, which could impact model accuracy.

In summary, this study provides a detailed picture of the structural and physiological changes that occur in the rabbit SSP after tenotomy and repair over time. We modeled a predicted length-tension curve based on these architectural data to reconcile structure with physiology. Through performing physiology testing, we assessed the length-tension relationship of each animal in each group, and we compare it with the predicted models. We report important physiological parameters, including the muscle strain, peak force, and peak stress in the muscle for each group. These findings elucidate key structural and physiological muscular changes after tenotomy and repair, which will allow researchers to better assess functional aspects of potential therapies for RC tear (8, 9, 15, 33).

Acknowledgements

This chapter, in full, is being prepared for submission for publication. Sydnee A Hyman, Isabella T Wu, Laura S Vasquez-Bolanos, Mackenzie B Norman, Shanelle N Dorn, Shannon N Bremner, Mary C Esparza, Ivan Ramirez, Donald C. Fithian, John G. Lane, Anshuman Singh, Samuel R Ward. The dissertation author is the primary investigator of this work.

Figures

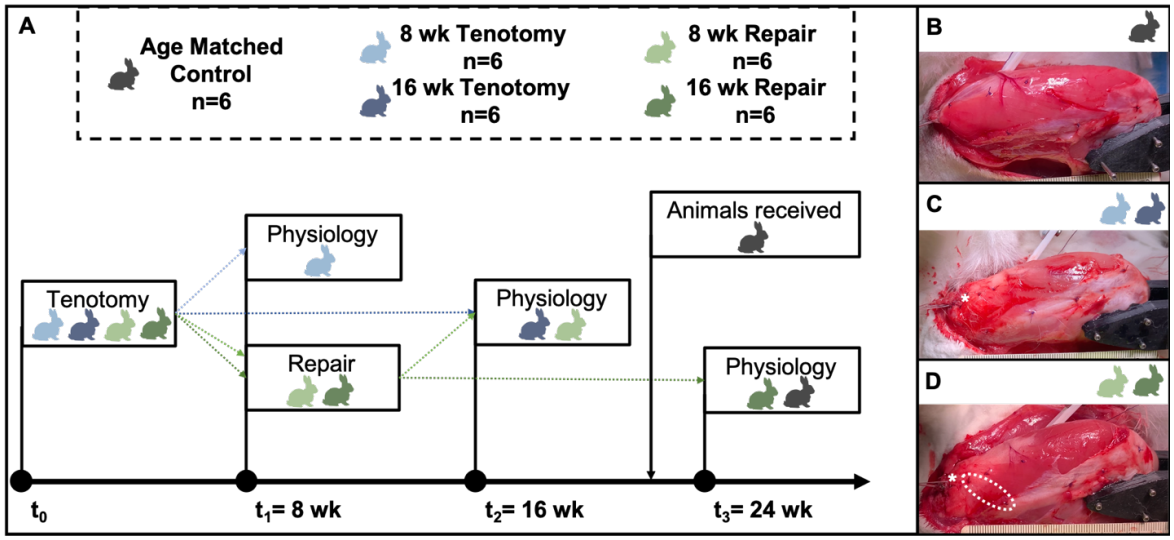

Figure 3.1 Experimental design. Timeline for generating each experimental group (A). Representative images during the physiology experiment for each experimental group (B-D). The age matched control animals show healthy muscle tissue (B); tenotomy showing atrophy, fat accumulation, and muscle retraction at the myotendinous (MT) junction (C, MT junction indicated by *); and repair showing fat (*) and shortened muscle fibers (dotted region) at the myotendinous junction (D).

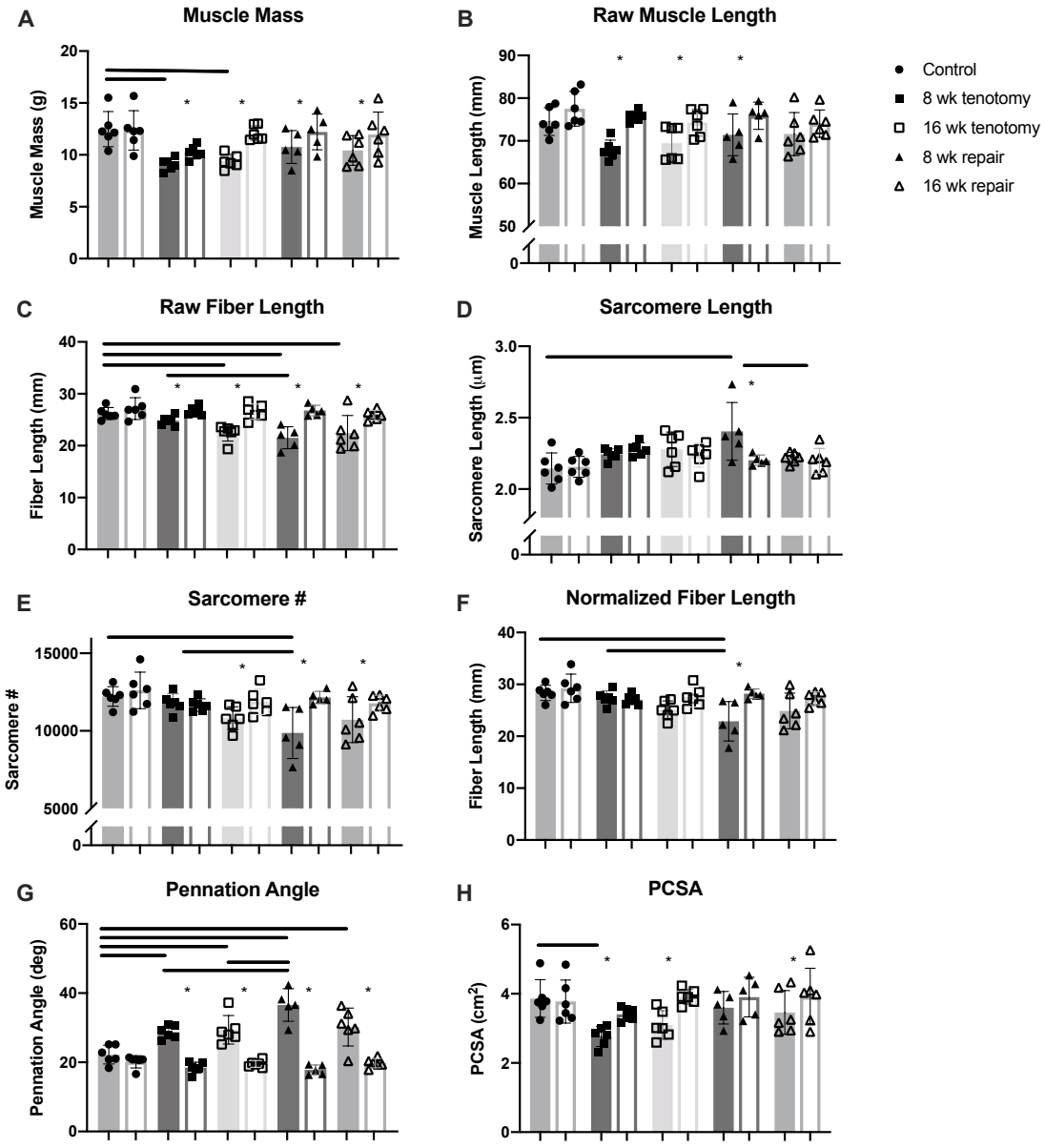

Figure 3.2 Architectural changes following tenotomy and repair. Average mass and raw muscle length (A and B), raw fiber length and sarcomere length (C and D), sarcomere number and normalized fiber length (E and F), pennation angle and PCSA (G and H) for rabbit SSP shown for each group. The experimental side (filled bars) and contralateral internal control (open bars) are shown (n=6/group for control, 8 wk tenotomy, 16 wk tenotomy, and 16 wk repair; n=5 for 8 wk repair). Bars indicate mean ± SD. Data was analyzed with two-way ANOVA ($p < 0.05$), using *post-hoc* Sidak's test to compare intervention groups, and Fischer's LSD test to compare contralateral vs. experimental side differences.

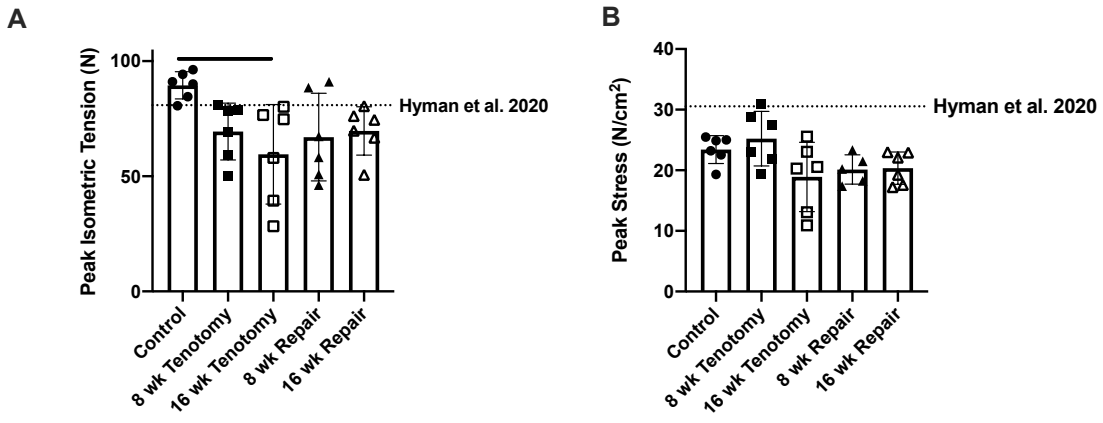

Figure 3.3 Peak isometric force (A) and stress (B) per animal (N=30, n=6 rabbits per group except 8 wk repair Peak Stress, which has n=5). Dotted line shows values from previously published study on 6-month old NZ white rabbit SSP (16). Peak isometric force is significantly decreased after 16 wk tenotomy, compared to controls. Each point represents one animal, and bars are shown as mean ± SD. Data analyzed with one-way ANOVA and post-hoc Tukey's test ($p < 0.05$).

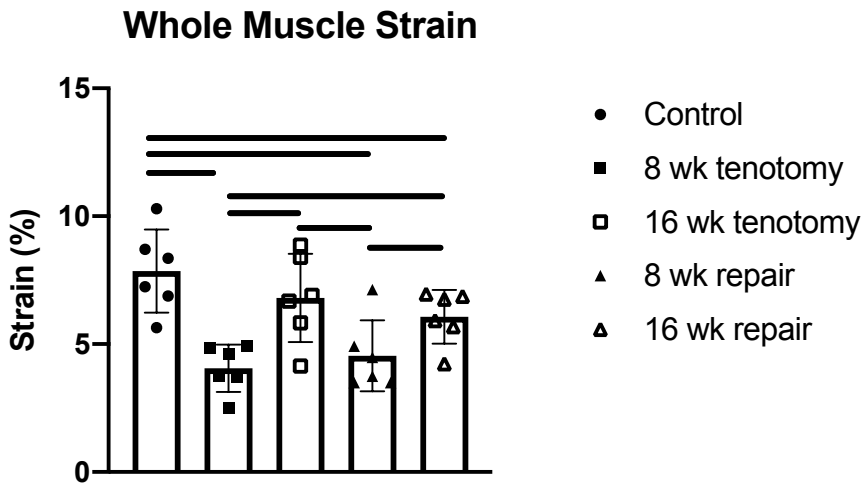

Figure 3.4 Whole muscle strain per animal (N=30, n=6 rabbits per group). Compared to controls, muscle strain was significantly lower after 8 wk tenotomy, 8 wk repair, and 16 wk repair. 8 wk tenotomy was significantly lower than 16 wk tenotomy and 16 wk repair. 16 wk tenotomy was significantly higher than 8 wk repair. 8 wk repair was significantly lower than 16 wk repair. Significance shown with horizontal lines. Each point represents one animal, and bars are shown as mean ± SD. Data analyzed with one-way ANOVA and post-hoc Tukey's test ($p < 0.05$).

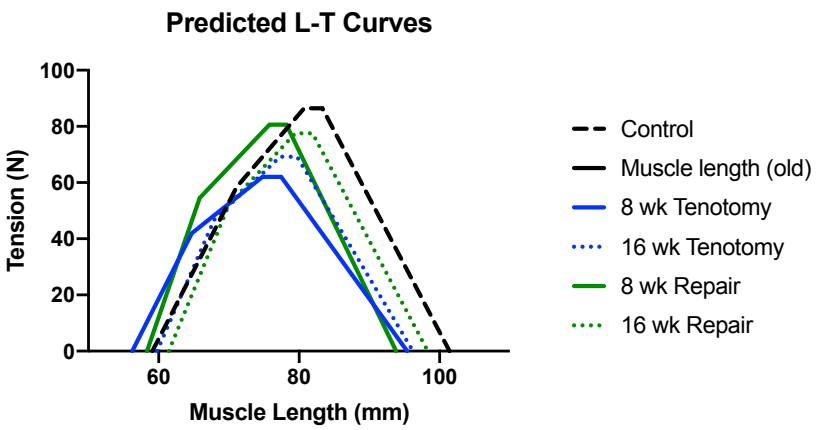

Figure 3.5 Predicted Length-Tension Curves for each experimental group.

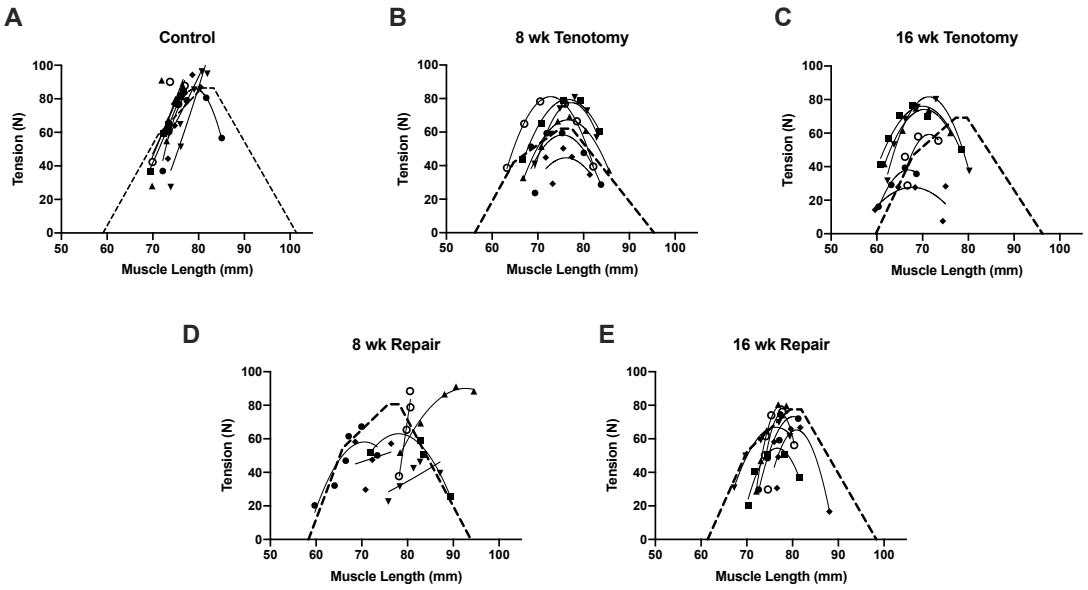

Figure 3.6 Predicted length-tension curves (dashed line) and individual data points fitted with second order polynomial regressions for each rabbit in each experimental group. Each point represents one contraction with different symbols used for each animal (N = 30, n = 6 female rabbits/group).

Supplemental Material

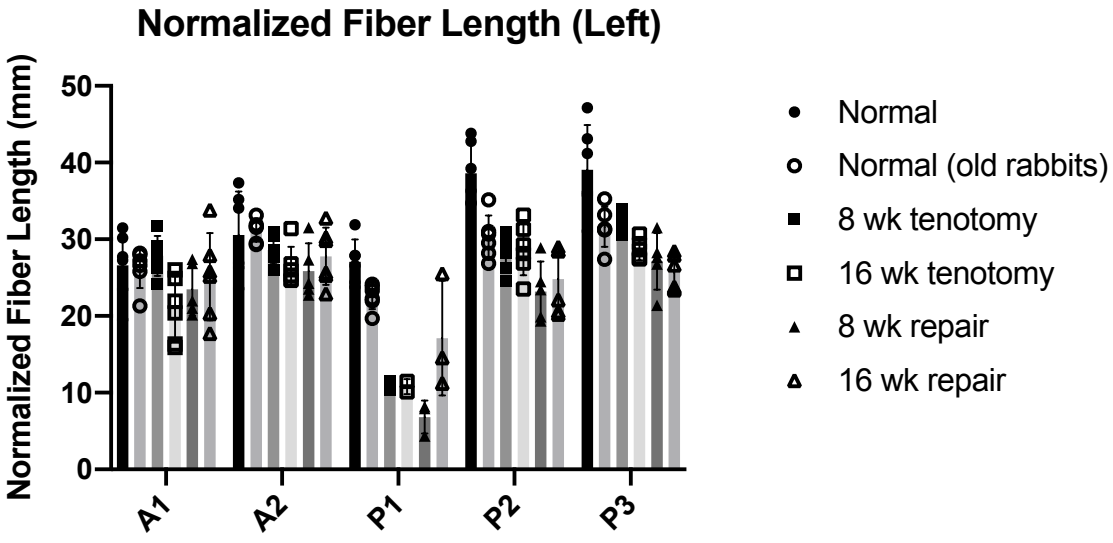

Figure 3.7S Regional differences in normalized fiber length. The experimental side is shown (n=6/group for control, 8 wk tenotomy, 16 wk tenotomy, and 16 wk repair; n=5 for 8 wk repair). Bars indicate mean ± SD.

Table 3.2S Comparison of experimental vs. predicted curve width

Curve Width (Full Width at Half Max, mm)										
	Control		8 wk Tenotomy		16 wk Tenotomy		8 wk Repair		16 wk Repair	
	Exp.	Pred.	Exp.	Pred.	Exp.	Pred.	Exp.	Pred.	Exp.	Pred.
Mean	13.79	29.77	17.81	27.67	16.15	25.73	21.19	25.09	13.17	26.02
Std. dev	1.02	1.14	1.60	1.05	3.11	1.32	5.75	3.05	2.15	2.68
p	<0.0001		0.0003		0.0003		0.4125		<0.0001	

Table 3.3S Comparison of experimental vs. predicted curve height

Curve Height (Peak Force, N)										
	Control		8 wk Tenotomy		16 wk Tenotomy		8 wk Repair		16 wk Repair	
	Exp.	Pred.	Exp.	Pred.	Exp.	Pred.	Exp.	Pred.	Exp.	Pred.
Mean	89.49	86.89	69.46	62.25	59.55	69.71	67.00	67.46	69.70	77.85
Std. dev	5.40	11.22	11.27	5.92	19.73	8.46	17.37	31.38	9.61	12.97
p	0.9996		0.9533		0.8285		>0.9999		0.9236	

Table 3.4S Comparison of experimental vs. predicted optimal muscle length

	Optimal muscle length (mm)									
	Control		8 wk Tenotomy		16 wk Tenotomy		8 wk Repair		16 wk Repair	
	Exp.	Pred.	Exp.	Pred.	Exp.	Pred.	Exp.	Pred.	Exp.	Pred.
Mean	78.67	80.71	75.81	74.80	69.63	77.28	81.23	75.78	78.48	79.45
Std. dev	1.94	4.90	1.47	4.39	1.74	3.39	8.07	9.38	1.68	3.98
p	0.9643		0.9986		0.0569		0.4540		0.9988	

References

1. Collin P, Thomazeau H, Walch G, Gerber C, Mansat P, Favard L, Colmar M, Kempf JF, Herve A, Betz M. Clinical and structural outcome twenty years after repair of isolated supraspinatus tendon tears. *J Shoulder Elbow Surg* 28: 196–202, 2019. doi: 10.1016/j.jse.2018.07.023.

2. Davis ME, Stafford PL, Jergenson MJ, Bedi A, Mendias CL. Muscle Fibers are Injured at the Time of Acute and Chronic Rotator Cuff Repair. *Clin Orthop* 473: 226–232, 2015. doi: 10.1007/s11999-014-3860-y.

3. Fabis J, Kordek P, Bogucki A, Mazanowska-Gajdowicz J. Function of the rabbit supraspinatus muscle after large detachment of its tendon: 6-week, 3-month, and 6-month observation. *J Shoulder Elbow Surg* 9: 211–6, 2000.

4. Farshad M, Meyer DC, Nuss KMR, Gerber C. A modified rabbit model for rotator cuff tendon tears: functional, histological and radiological characteristics of the supraspinatus muscle. *Shoulder Elb* 4: 90–94, 2012. doi: 10.1111/j.1758-5740.2011.00170.x.

5. Feeley BT, Liu M, Ma CB, Agha O, Aung M, Lee C, Liu X. Human Rotator Cuff Tears Have an Endogenous, Inducible Stem Cell Source Capable of Improving Muscle Quality and Function After Rotator Cuff Repair. .

6. Gerber C, Meyer DC, Nuss KM, Farshad M. Anabolic steroids reduce muscle damage caused by rotator cuff tendon release in an experimental study in rabbits. *J Bone Joint Surg Am* 93: 2189–2195, 2011. doi: 10.2106/JBJS.J.01589.

7. Gerber C, Meyer DC, Schneeberger AG, Hoppeler H, Rechenberg BV. Effect of Tendon Release and Delayed Repair on the Structure of the Muscles of the Rotator Cuff: An Experimental Study in Sheep. *J Bone Joint Surg Am* 86:1973-1982, 2004.

8. Gerber C, Schneeberger AG, Beck M, Schlegel U. Mechanical strength of repairs of the rotator cuff. *J Bone Jt Surg Br* 76: 371–80, 1994.

9. Gerber C, Schneeberger AG, Hoppeler H, Meyer DC. Correlation of atrophy and fatty infiltration on strength and integrity of rotator cuff repairs: a study in thirteen patients. *J Shoulder Elbow Surg* 16: 691–696, 2007. doi: 10.1016/j.jse.2007.02.122.

10. Gibbons MC, Sato EJ, Bachasson D, Cheng T, Azimi H, Schenk S, Engler AJ, Singh A, Ward SR. Muscle architectural changes after massive human rotator cuff tear. *J Orthop Res* 34: 2089–2095, 2016. doi: 10.1002/jor.23256.

11. Gibbons MC, Singh A, Anakwenze O, Cheng T, Pomerantz M, Schenk S, Engler AJ, Ward SR. Histological Evidence of Muscle Degeneration in Advanced Human Rotator Cuff Disease. *J Bone Jt Surg Am* 99: 190–199, 2017. doi: 10.2106/jbjs.16.00335.

12. Gladstone JN, Bishop JY, Lo IKY, Flatow EL. Fatty infiltration and atrophy of the rotator cuff do not improve after rotator cuff repair and correlate with poor functional outcome. *Am J Sports Med* 35: 719–728, 2007. doi: 10.1177/0363546506297539.

13. Goutallier D, Postel J-M, Gleyze P, Leguilloux P, Van Driessche S. Influence of cuff muscle fatty degeneration on anatomic and functional outcomes after simple suture of full-thickness tears. *J Shoulder Elbow Surg* 12: 550–554, 2003. doi: 10.1016/s1058-2746(03)00211-8.

14. Gumucio JP, Davis ME, Bradley JR, Stafford PL, Schiffman CJ, Lynch EB, Claflin DR, Bedi A, Mendias CL. Rotator cuff tear reduces muscle fiber specific force production and induces macrophage accumulation and autophagy. *J Orthop Res Off Publ Orthop Res Soc* 30: 1963–1970, 2012. doi: 10.1002/jor.22168.

15. Hersche O, Gerber C. Passive tension in the supraspinatus musculotendinous unit after long-standing rupture of its tendon: A preliminary report. *J Shoulder Elbow Surg* 7: 393–396, 1998. doi: 10.1016/S1058-2746(98)90030-1.

16. Hyman SA, Norman MB, Dorn SN, Bremner SN, Esparza MC, Lieber RL, Ward SR. In Vivo Supraspinatus Muscle Contractility and Architecture in Rabbit. .

17. Lieber R. *Skeletal muscle structure, function, and plasticity*. 2011.

18. Lieber RL, Friden J. Functional and clinical significance of skeletal muscle architecture. *Muscle Nerve* 23: 1647-1666, 2000.

19. Lieber RL, Yeh Y, Baskin RJ. Sarcomere length determination using laser diffraction. Effect of beam and fiber diameter. *Biophys J* 45: 1007–1016, 1984.

20. Mathewson MA, Kwan A, Eng CM, Lieber RL, Ward SR. Comparison of rotator cuff muscle architecture between humans and other selected vertebrate species. *J Exp Biol* 217: 261–273, 2014. doi: 10.1242/jeb.083923.

21. Matsumoto F, Uhthoff HK, Trudel G, Loehr JF. Delayed tendon reattachment does not reverse atrophy and fat accumulation of the supraspinatus--an experimental study in rabbits. *J Orthop Res Off Publ Orthop Res Soc* 20: 357–363, 2002. doi: 10.1016/S0736-0266(01)00093-6.

22. McCracken TO, Kainer RA, Carlson D. Color Atlas of Small Animal Anatomy: The Essentials, Revised Edition [Online]. Wiley-Blackwell. https://www.wiley.com/en-us/Color+Atlas+of+Small+Animal+Anatomy%3A+The+Essentials%2C+Revised+Edition-p-9780813816081 [24 Aug. 2020].

23. Mendias CL, Roche SM, Harning JA, Davis ME, Lynch EB, Sibilsky Enselman ER, Jacobson JA, Claflin DR, Calve S, Bedi A. Reduced muscle fiber force production and disrupted myofibril architecture in patients with chronic rotator cuff tears. *J Shoulder Elbow Surg* 24: 111–119, 2015. doi: 10.1016/j.jse.2014.06.037.

24. Meyer DC, Gerber C, Von Rechenberg B, Wirth SH, Farshad M. Amplitude and Strength of Muscle Contraction Are Reduced in Experimental Tears of the Rotator Cuff. *Am J Sports Med* 39: 1456–1461, 2011. doi: 10.1177/0363546510396305.

25. Meyer DC, Hoppeler H, Rechenberg B von, Gerber C. A pathomechanical concept explains muscle loss and fatty muscular changes following surgical tendon release. *J Orthop Res* 22: 1004–1007, 2004. doi: 10.1016/j.orthres.2004.02.009.

26. Petersen SA, Murphy TP. The timing of rotator cuff repair for the restoration of function. *J Shoulder Elbow Surg* 20: 62–68, 2011. doi: 10.1016/j.jse.2010.04.045.

27. Rubino LJ, Stills HF, Sprott DC, Crosby LA. Fatty infiltration of the torn rotator cuff worsens over time in a rabbit model. *Arthrosc J Arthrosc Relat Surg Off Publ Arthrosc Assoc N Am Int Arthrosc Assoc* 23: 717–722, 2007. doi: 10.1016/j.arthro.2007.01.023.

28. Sacks RD, Roy RR. Architecture of the hind limb muscles of cats: Functional significance. *J Morphol* 173: 185–195, 1982. doi: 10.1002/jmor.1051730206.

29. Schindelin J, Arganda-Carreras I, Frise E, Kaynig V, Longair M, Pietzsch T, Preibisch S, Rueden C, Saalfeld S, Schmid B, Tinevez J-Y, White DJ, Hartenstein V, Eliceiri K, Tomancak P, Cardona A. Fiji: an open-source platform for biological-image analysis. *Nat Methods* 9: 676–682, 2012. doi: 10.1038/nmeth.2019.

30. Shen P-H, Lien S-B, Shen H-C, Lee C-H, Wu S-S, Lin L-C. Long-term functional outcomes after repair of rotator cuff tears correlated with atrophy of the supraspinatus muscles on magnetic resonance images. *J Shoulder Elbow Surg* 17: 1S-7S, 2008. doi: 10.1016/j.jse.2007.04.014.

31. Tomioka T, Minagawa H, Kijima H, Yamamoto N, Abe H, Maesani M, Kikuchi K, Abe H, Shimada Y, Itoi E. Sarcomere length of torn rotator cuff muscle. *J Shoulder Elbow Surg* 18: 955–9, 2009. doi: 10.1016/j.jse.2009.03.009.

32. Uhthoff HK, Matsumoto F, Trudel G, Himori K. Early reattachment does not reverse atrophy and fat accumulation of the supraspinatus--an experimental study in rabbits. *J Orthop Res Off Publ Orthop Res Soc* 21: 386–392, 2003. doi: 10.1016/S0736-0266(02)00208-5.

33. Valencia AP, Lai JK, Iyer SR, Mistretta KL, Spangenburg EE, Davis DL, Lovering RM, Gilotra MN. Fatty Infiltration Is a Prognostic Marker of Muscle Function After Rotator Cuff Tear. *Am J Sports Med* 46: 2161–2169, 2018. doi: 10.1177/0363546518769267.

34. Ward SR, Hentzen ER, Smallwood LH, Eastlack RK, Burns KA, Fithian DC, Friden J, Lieber RL. Rotator cuff muscle architecture: implications for glenohumeral stability. *Clin Orthop* 448: 157–63, 2006. doi: 10.1097/01.blo.0000194680.94882.d3.

35. Ward SR, Lieber RL. Density and hydration of fresh and fixed human skeletal muscle. *J Biomech* 38: 2317–2320, 2005. doi: 10.1016/j.jbiomech.2004.10.001.

36. Wilde JM, Gumucio JP, Grekin JA, Sarver DC, Noah AC, Ruehlmann DG, Davis ME, Bedi A, Mendias CL. Inhibition of p38 MAPK Signaling Reduces Fibrosis and Lipid Accumulation After Rotator Cuff Repair. *J Shoulder Elb Surg Am Shoulder Elb Surg Al* 25: 1501–1508, 2016. doi: 10.1016/j.jse.2016.01.035.

37. Winters TM, Takahashi M, Lieber RL, Ward SR. Whole muscle length-tension relationships are accurately modeled as scaled sarcomeres in rabbit hindlimb muscles. *J Biomech* 44: 109–115, 2011. doi: 10.1016/j.jbiomech.2010.08.033.

Chapter 4. Exercise-related Signaling Is not Impacted by Supraspinatus Tear or Repair in Rabbit

Abstract

Atrophic muscle changes related to chronic rotator cuff (RC) tear are both difficult to treat clinically and associated with poor clinical outcomes. Decreased muscle quality (atrophy, retraction, fibrosis, and fatty infiltration) persists even after successful surgical repair; consequently, current therapies are focused on slowing progression of atrophy and fatty infiltration rather than reversal of these pathologic processes. With the lack of hypertrophic response during recovery after surgery, mechanotransduction pathways may be implicated, as a loss in sensitivity to mechanical stimulus could explain the lack of muscle recovery after repair. We utilized a New Zealand white rabbit model of supraspinatus tenotomy and repair (N=18, n=6 control, 16 wk tenotomy, 16 wk repair). Under 2% isofluorane anesthesia, we generated isometric contractions (first, a length-tension experiment, followed by two series of 10 contractions) and assessed the activation of JNK and p38 MAPKs at two timepoints following the exercise bout. Despite the structural changes in the muscle after tear and repair, muscle stress was not different between groups. This allowed us to compare the basal levels of phosphorylated JNK and p38, fold changes in phosphorylation of JNK and p38, and changes in total JNK and p38 after the contractions. There was a significant increase in pJNK and p-p38 fold-change across all groups, but no differences in fold change of pJNK or p-p38 between groups were observed. Overall, these findings indicate that acute activation of JNK and p38 MAPKs are not inhibited in a chronic tenotomy or repair model of RC disease.

Introduction

Chronic rotator cuff (RC) disease results in decreased muscle quality, characterized by muscle atrophy, fibrosis, and fatty infiltration (5, 12). These gross muscle changes are accompanied by

downregulation of hypertrophic and upregulation of atrophic, fibrotic, and adipogenic genes in humans (3, 10, 11), sheep (7, 27), and rodents (16, 23). Decreased muscle quality persists despite surgical intervention and physical therapy, leading to significant clinical problems (5, 9, 12, 15, 29).

In healthy muscle, exercise activates hypertrophic signaling pathways, while inhibiting atrophic signaling through several axes (13, 18, 28). For example, increased phosphorylation of c-Jun NH_2-terminal kinase (JNK) and p38 mitogen activated protein kinase (MAPK) are robust markers of muscle "activation" in response to mechanical stress, and their phosphorylation increases in a tension-dependent manner (2, 8, 22, 24, 30). Downstream effects of activation of this pathway has been linked to mRNA modulation of pro-hypertrophic genes (e.g. mTOR, myostatin, and p70s6k) (6, 17, 21, 22). The inhibition of p38 MAPK signaling at the time of repair reduced muscle atrophy in a rat model, suggesting an important role in RC disease progression (33). While no studies have explicitly explored JNK's role in the decrease of RC muscle quality, it plays a key role in responding to skeletal muscle stress (8, 22). Because of the persistent muscle loss and fatty infiltration that occurs in RC disease (5, 14), even in response to physical therapy after successful surgical repair (12), we hypothesized that p38 MAPK and JNK signaling, and hypertrophy-related mRNA expression, in response to a mechanical stress would be highest in normal, lowest in chronically torn, and slightly improved in the surgically repaired muscles. To test this hypothesis, we utilized a rabbit model of RC tear and repair, as well as a validated muscle physiology experimental preparation (19), to investigate p38 and JNK signaling in normal, chronically torn, and surgically repaired RC muscles acutely after a contractile stimulus (referred to as the exercise bout).

Materials and Methods

Animals: All experimental procedures were approved by the Institutional Animal Care and Use Committee (IACUC) of the University of California, San Diego. Eighteen skeletally mature female New Zealand white rabbits (n=6/group) were used for this study. The animals used for intervention groups (16

wk tenotomy and 16 wk repair) were 6 months old at the beginning of the study. To account for animal growth over the course of the study, control rabbits were age-matched to the final age of the intervention group rabbits, roughly 1 year old (Fig. 4.1A). Mean body weight at sacrifice was 4.36±0.50 kg, 4.30±0.17 kg, and 4.24±0.34 kg for the age-matched control, 16 wk tenotomy, and 16 wk repair groups, respectively.

Cage locations were assigned upon arrival, each rabbit was given a number ID, and then randomized to one of the study groups. Researchers were aware of the allocation during the surgeries and tissue harvest, but the specimens were identified by ID number only. Animals were single-housed with food and water ad lib, environmental and food enrichment, and visual access to other animals. There were no adverse events in this study and no animals met the criteria for humane endpoints. These criteria included: displaying clinical signs of disease, loss of appetite, weight below 15% of what is expected for the animal, and/or signs of distress, such as self-mutilation.

Surgical Procedures: For all surgical procedures, rabbits were anesthetized with a subcutaneous injection of a ketamine-xylazine cocktail (50 and 5 mg/kg body mass, respectively) and maintained on 2% isoflurane anesthesia. Heart rate and oxygen saturation were monitored (VetOx, Heska Co., Fort Collins, CO) throughout the test duration. The left supraspinatus (SSP) muscle served as the experimental side in all animals, with the contralateral shoulder as an unoperated internal control.

All intervention groups underwent the following tenotomy procedure. An open anterior approach was performed on the left shoulder, followed by sharp transection of the left SSP tendon from its footprint on the greater tuberosity of the humerus. The surrounding soft tissues were bluntly dissected to allow unhindered retraction of the tendon stump and distal muscle. After securing a Penrose drain to the tendon stump to prevent scar formation between the tendon and surrounding soft tissue, the incision was closed in layers.

The repair group underwent the following SSP repair procedure 8 weeks after tenotomy. Using the same anesthesia and anterior approach as the tenotomy, the repair was performed using a modified locking suture with anterior and posterior bone tunnels to restore the tendon footprint to the humeral head. Fibrous adhesions and any remaining tendon stump on the greater tubercle of the humerus was scraped away to allow for tendon-to-bone healing after SSP repair. Closure and post-operative protocols were the same as above. Rabbits were then allowed individual cage activity with routine post-operative care. Buprenorphine SR was used for analgesia, and the animals were monitored daily for 2 weeks post-operatively.

All animals underwent the following procedure to test the length-tension relationship in the SSP using methods previously described (19). Briefly, under anesthesia, an open approach was used to expose the SSP by dividing the middle trapezius and deltoid muscles. The suprascapular nerve was isolated by blunt dissection around the anterior aspect of the SSP (25), and a cuff electrode (Pulsar 6Bp Stimulator; FHC, Bowdoinham, ME) was placed around the nerve for direct stimulation. The distal SSP tendon was transected, released from the superior joint capsule, sutured to a servomotor (Cambridge Model 310B; Aurora Scientific, Aurora, ON, Canada), and aligned with the force-generating axis of the motor. Muscle temperature was maintained at 37°C with radiant heat, heated saline, and a servo-temperature controller (Model 73A; YSI, Yellow Springs, OH). A custom-built clamp was used to immobilize the scapula, placed from the vertebral border along the scapular spine on top of the infraspinatus fossa.

Exercise protocol: First, the length-tension protocol (Fig. 4.1B) was performed as previously described (19). Briefly, a series of 100 Hz tetanic contractions (pulse width: 0.3 ms; amplitude: 10 V) over a 640 ms period were delivered every two minutes. The first contraction was performed with the muscle set to its neutral length (the muscle length measured at 90° joint angle). For each subsequent contraction, the servomotor position was advanced 5 mm to lengthen the muscle. This was repeated until

the muscle was operating on the descending limb of the length-tension curve, with a minimum of four contractions per animal.

After this was performed, muscle length was set to optimal length (the recorded length that yielded maximal contraction), and two series of ten tetanic contractions (pulse width: 0.3 ms; amplitude: 7 V) were delivered. Each contraction was 30sec apart, and each series was two minutes apart. Two rabbits in the Control group did not undergo these two sets of 10 contractions, and they were omitted from the analysis of the exercise bout.

Muscle Biopsies: Muscle biopsies were taken (~20mg each; 6 biopsies total: two muscle regions at three time points) over the course of the experiment (Fig. 4.1B). Muscle fascicles were carefully dissected to minimize mechanical stress (compression and stretch) on the fibers for biopsy selection. Biopsies were immediately snap-frozen in liquid nitrogen and later transferred to a -80C freezer for later sample preparation. The first biopsy (Pre) was taken as soon as the SSP was surgically exposed. Immediately after the second series of "exercise" contractions were performed, the Post 0 biopsy was taken. Following a 30-minute period where the animal was kept under anesthesia before euthanasia, the Post 30 biopsy was taken. The two rabbits that did not undergo the two sets of 10 contractions were not included in the Post 0 and Post 30 analysis.

Homogenization and Sample Preparation: Frozen SSP biopsies were powdered using a Cellcrusher tissue pulverizer on dry ice and homogenized in 10-fold mass ice-cold lysis buffer [50 mM Tris, 1 mM EDTA, 1 mM EGTA, 50 mM NaF, 5 mM $Na_4P_2O_7$-$10H_2O$, 270 mM sucrose, 1 M Triton-X, 25 mM β-glycerophosphate, 1 μM trichostatin A, 10 mM nicotinamide, 1 mM 1,4-dithiothreitol, 1% phosphatase inhibitor cocktail 2 (Sigma-Aldrich), 1% phosphatase inhibitor cocktail 3 (Sigma-Aldrich),

4.8% cOmplete mini protease inhibitor cocktail (Roche Applied Science)]. Samples were then rotated end over end for 2 h, centrifuged at 4°C for 10 min at 8,000 *g* and the supernatant was collected. Supernatant protein concentrations were quantified via bicinchoninic acid method (Pierce BCA Protein Assay Reagent A #23223, Reagent B #23224, 660nm Protein Assay Reagent #22660) and then samples were prepped at the same protein concentration (0.8 mg/mL) in 1 × Laemmli sample buffer.

Immunoblotting: After boiling for 5 min at 100ºC, equal amounts of protein (20 µg) were separated on XT criterion precast gels (3-8% Tris-Acetate, 18 well gels, Bio-Rad Laboratories) under reducing conditions and were then transferred to Amersham Protran nitrocellulose membranes (Millipore Sigma). The nitrocellulose membranes were stained with ponceau S solution (0.1% [wt/vol] ponceau S in 5% acetic acid), imaged (ChemiDoc XRS$^+$, Bio-Rad Laboratories) and washed with 1X TBST. Next, the membranes were blocked with 5% milk in TBST for 1 hour at room temperature. The membranes were then incubated with primary antibodies overnight in 4°C. The following primary antibodies from Cell Signaling Technology were diluted 1:1000 in 5% BSA: p38 MAPK (CS 9212), phospho-p38 MAPK (Thr180/Tyr182) (p-p38; CS 9211), JNK/SAPK (CS 9252), phospho-JNK/SAPK (T183/Y185) (pJNK; CS 9251), and eukaryotic elongation factor 2 (eEF2; CS 2332). Following the overnight primary antibody incubation, membranes were incubated in appropriate secondary antibodies (diluted 1:10,000 in 5% milk in TBST) for 1 hour. The blots were developed and imaged (ChemiDoc XRS$^+$, Bio-Rad Laboratories) utilizing a chemiluminescent substrate to detect horseradish peroxidase. Densitometric analysis of immunoblots was performed using Image Lab Software 6.1 (Bio-Rad Laboratories). Total protein was normalized to eEF2, and phosphorylated protein was normalized to total abundance.

Data Analysis: One sample t-tests were used to compare the fold changes in phosphorylation/total protein levels for JNK and p38 across all groups immediately after (post 0) and 30 minutes after (post 30)

the exercise bout (hypothetical mean = 1, $p < 0.05$). One-way ANOVA with *post-hoc* Tukey's tests were used to compare physiological parameters between groups. Two-way repeated measures ANOVA and *post-hoc* Tukey's tests were used to compare cell signaling data for main effects (time) and simple effects between groups and within groups. One-way ANOVA with *post-hoc* Tukey's test was used to compare the basal ratios of phosphor/total protein relative to the control group. Linear regressions were used to correlate cell signaling response (fold change in phosphor/total protein immediately after exercise bout) to physiological parameters. Significance for all analyses was set at $p < 0.05$, and data are presented as mean ± SD.

Results

Force production was impaired after tenotomy. Peak isometric tension (Fig. 4.2A) was significantly decreased after tenotomy (59.6±19.70 N vs. 89.4±5.40 N), and it was not significantly improved after repair (69.7±9.61 N). The coefficient of variation for force production in the tenotomy group was highest (33%). Muscle stress (Fig. 4.2B) was not statistically different between groups, although there were two animals in the tenotomy group with low peak stress (~11N/cm^2). Whole muscle strain (Fig. 4.2C) is significantly lower after repair compared to controls (6.1% vs. 7.9%), but not significant after tenotomy (6.8%).

Exercise stimulus was consistent between groups. There was a 25% decrease in average peak tension (Fig. 4.3A) after tenotomy that did not recover after repair, but this did not achieve statistical significance ($p = 0.25$ and 0.27, respectively). The number of contractions (Fig. 4.3B) between groups was not significantly different. There was downward trend of 33% in the sum of the force time integral (Fig. 4.3C) after tenotomy ($p = 0.08$) that did not significantly increase after repair (1003±244, 673±230, 717±180 N s for control, tenotomy, and repair, respectively). Statistical power for comparing the average

peak tension and force time integral were 0.43 and 0.73, respectively. Two rabbits in the Control group did not undergo these two sets of 10 contractions, and they were omitted from the analysis of the exercise bout.

Acute signaling response to contractile stimulus (exercise bout). Signaling results were quantified from the gels (Fig. 4.4). There were significant differences in the fold change of phosphorylated/total JNK and p38 ($p = 0.018$, $p = 0.020$, respectively) immediately after the exercise bout (Fig. 4.5A and B). 30 minutes after the contractions, fold change in phospho/total JNK and p38 are not significantly increased over pre-contraction.

There were no differences in basal levels of phosphorylated JNK or p38, regardless of group (Fig. 4.6A and D, respectively). Immediately after the contractions, there was a 2.04±1.90, 1.51±0.38, and 2.06±1.51 fold change in JNK phosphorylation for control, tenotomy, and repair groups, respectively (Fig. 4.6B), and these changes were not different between groups. Fold change in JNK phosphorylation was significantly increased for the tenotomy group compared to pre-contractions ($p = 0.049$) (Fig. 4.6B). After 30 min of rest, pJNK/tota lJNK was 2.06±2.50, 2.53±2.81, and 1.28±0.99 fold increased from pre-contraction levels (Fig. 4.6B), but this did not achieve statistical significance.

Immediately after the contractions, there were 2.07±.0.92, 5.31±5.55, 2.40±1.71 fold changes in p38 phosphorylation for control, tenotomy, and repair groups, respectively (Fig. 4.6E), and there were no significant differences between groups. 30 minutes after the contractions, p-p38 was significantly lower than immediately post-exercise for the control animals (Fig. 4.6E). After 30 min of rest, p-p38/total p38 was 1.03±1.02, 2.56±2.29, and 1.24±1.29 fold increased from pre-contraction levels (Fig. 4.6B), but this did not achieve statistical significance.

There was a significant decrease in total JNK/eEF2 from post 0 to post 30 across groups ($p = 0.049$) (Fig. 4.6C). There was also a significant difference in total p38/eEF2 over time ($p < 0.05$), but multiple comparisons showed no significant differences between timepoints (Fig. 4.6F).

Relationship between cell signaling response and exercise. No significant correlations were found between the fold change in phospho/total JNK or p38 immediately post exercise with respect to average tension (Fig. 4.7A and D), number of contractions (Fig. 4.7B and E), or the total force time integral for each animal (Fig. 4.7C and F).

Discussion

The objective of this study was to determine if chronic tenotomy and/or repair influences the SSP's cell signaling response to a contractile stimulus. Our hypothesis that there would be lower phosphorylation of JNK and p38 in the tenotomized and repaired muscles compared to control muscles was refuted, as there was a similar fold change increase in phosphorylation after contraction regardless of group. Despite the 33% lower peak force production for tenotomy and 25% reduced force production for repair (Fig. 4.2A), peak muscle stresses are not significantly different. Similarly, there was a 25% reduction in average tension and 33% reduction in force-time integral after tenotomy (Fig. 4.3), that did not improve after repair. Since the muscles in the tenotomy and repair groups are achieving similar muscle stresses as the control rabbits, the effective "duty cycle" for each group is roughly the same, as the atrophied muscles in tenotomy and repair are able to achieve normal stress levels even though their overall force output is lower. We found increased phosphorylation of JNK and p38 across groups (Fig. 4.5), but there were no significant differences in basal levels of pJNK or p38 (Fig. 4.6B and E), and no significant differences in total JNK or p38 between groups (Fig. 4.6C and F). Taken together, this

indicates that the muscles are still behaving relatively normal in terms of MAPK mechanotransduction (4, 26)

Previously, a correlation has been established between JNK phosphorylation with increasing tension (8, 24), which was not explicitly supported here. However, Martineau and Gardinier (24) performed 300 isometric contractions over 5 minutes in in a rat plantaris muscles, as opposed to our ~25 contractions over 20 minutes. They observed ~10 fold changes in JNK phosphorylation, where we observed ~2-3. Considering the order of magnitude larger number of contractions, an order of magnitude increase in fold change would be consistent with their finding that phosphorylation scales with tension. While performing 300 contractions of the rabbit SSP likely would have yielded a larger fold change in phosphorylation of JNK and p38, it is not clinically relevant as a rehabilitation exercise regime (20, 31). Additionally, the risk of muscle failure (through suture pullout or myotendinous junction tear) is nontrivial, as two of the control animals failed before the exercise bout had begun.

The muscles after tenotomy and repair have a ~25-35% reduction in force production, but physiologically behave as their structure would predict (determined by peak muscle stress being consistent with prior literature) (4, 19, 26), so they are not acting “sick” physiologically. As such, it is reasonable that the MAPK pathway would be activated proportionally to force production similarly between groups. Although this study does not directly address the role of MAPKs in regulation of muscle hypertrophy, the activation of both JNK and p38 here are consistent with the hypothesis that MAPKs could relay pro-hypertrophic stimuli (1, 22, 24). Due to this link, the implication of JNK and p38 in RC disease (32, 33), and the apparent inability for RC disease muscles to recover from atrophy (5, 9, 12, 29), we wanted to test if muscle activation in response to a contractile stimulus was impaired after chronic tenotomy and repair RC. It was not impaired.

This study has several limitations. First, the high experimental variability within groups and relatively low sample sizes make statistical comparisons difficult, and the study would benefit from

greater sample size. Second, the temporal resolution for analyzing the signaling response was limited by maintaining anesthesia for the rabbits, which narrows our data acquisition to at most 30 minutes after exercise.

In summary, this study demonstrates that chronically torn and repaired SSP muscles are activated to similar levels as controls using a clinically relevant exercise regime. These findings indicate that while muscles undergo structural changes after tenotomy and repair, they perform physiologically similar to one another, and the activation of the MAPK pathway by JNK and p38 are not altered by tear or repair. These data will be useful for researchers investigating why muscle loss persists even after successful surgical RC repair and rehabilitation.

Acknowledgements

This chapter, in full, is a reprint of the material being prepared for submission for publication. Sydnee A Hyman, Ji Kang, Ji Park, Laura S Vasquez-Bolanos, Isabella T Wu, Mackenzie B Norman, Shanelle N Dorn, Shannon N Bremner, Mary C Esparza, Donald C. Fithian, John G. Lane, Anshuman Singh, Simon Schenk, Samuel R Ward. The dissertation author was the primary investigator of this material.

Figures

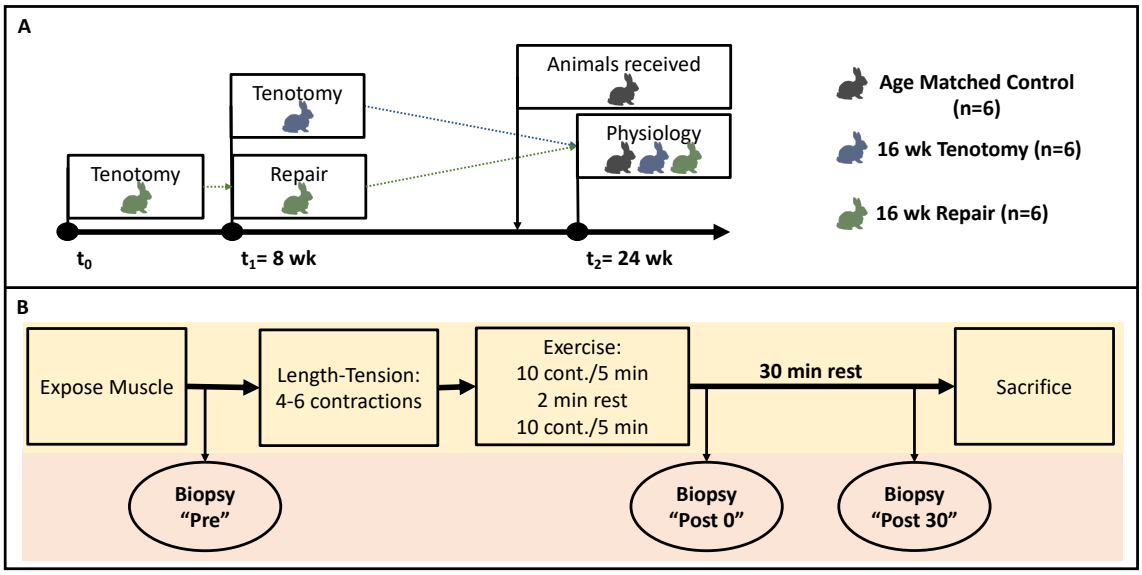

Figure 4.1. Experimental design (A) showing timeline for generating experimental groups. Flowchart for performing the physiology testing followed by the exercise bout and biopsy collection (B).

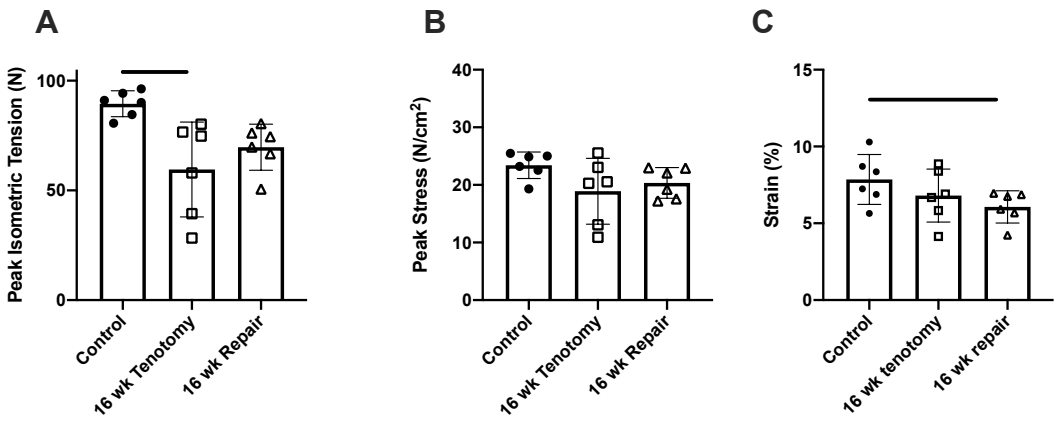

Figure 4.2. Physiological comparisons. Peak isometric force (A), stress (B), and whole muscle strain (C) are shown for each experimental group. Bars are mean ± SD. Data analyzed with one-way ANOVA and *post-hoc* Tukey's test (significance set at $p < 0.05$ and shown with lines).

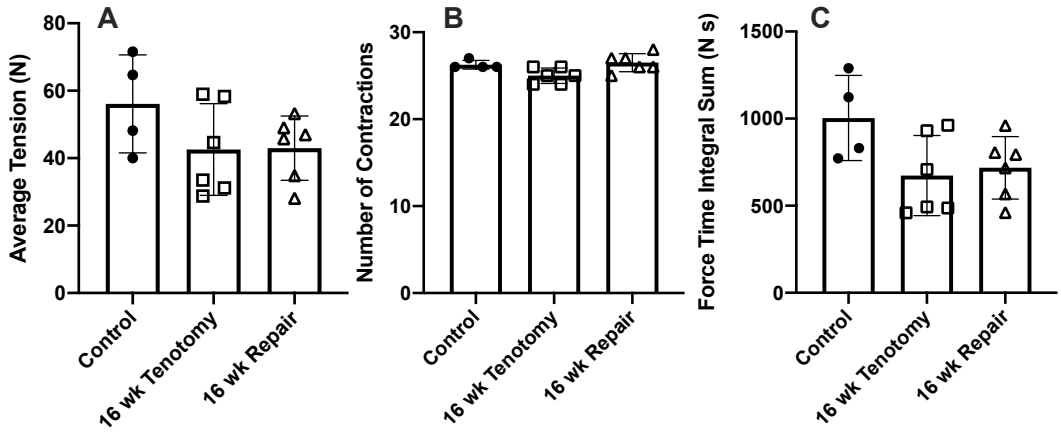

Figure 4.3. Characterization of exercise bout. Average tension for each animal (A), total number of contractions for each animal (B), and the sum of the force time integral for each animal (C) are shown for each experimental group. Bars are mean ± SD. Data analyzed with one-way ANOVA and *post-hoc* Tukey's test (significance set at $p < 0.05$).

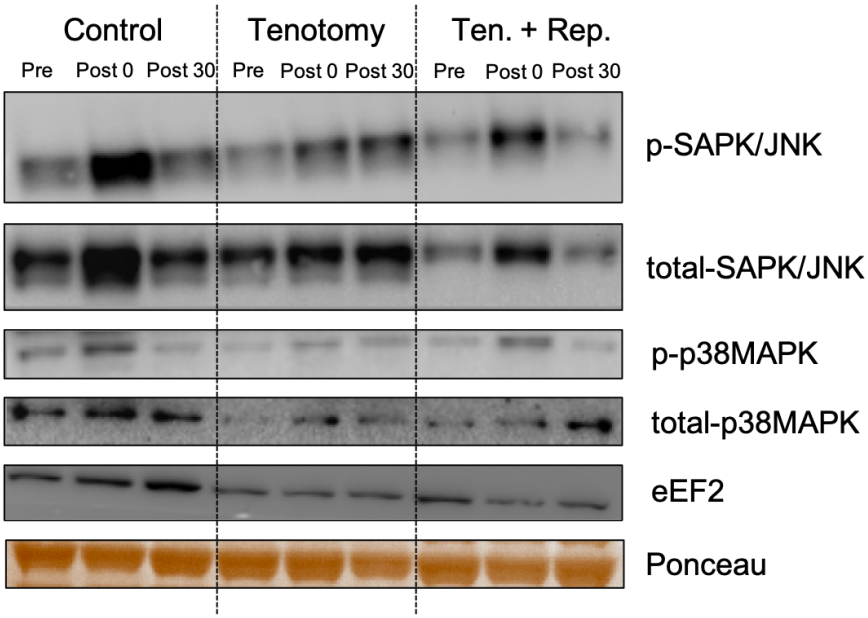

Figure 4.4 Representative immunoblots for each experimental group.

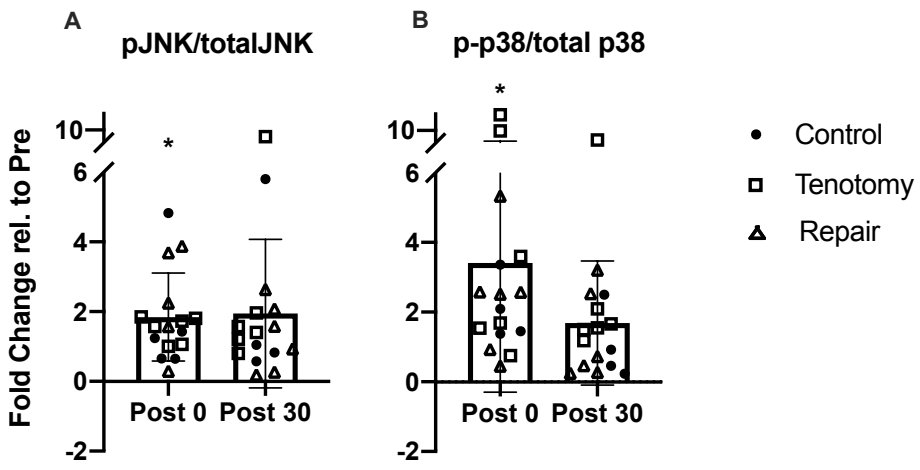

Figure 4.5. Fold changes in phosphorylation of JNK (A) and p38 (B) relative to pre-contraction over all groups (N=16; n=4 control, n=6 tenotomy, n=6 repair). Bars are mean ± SD. One-sample t tests were used to compare the fold changes in phosphorylation at Post 0 and Post 30 to Pre contraction compared to a hypothetical mean of 1. Significance was set at $p < 0.05$ and is shown with asterisks.

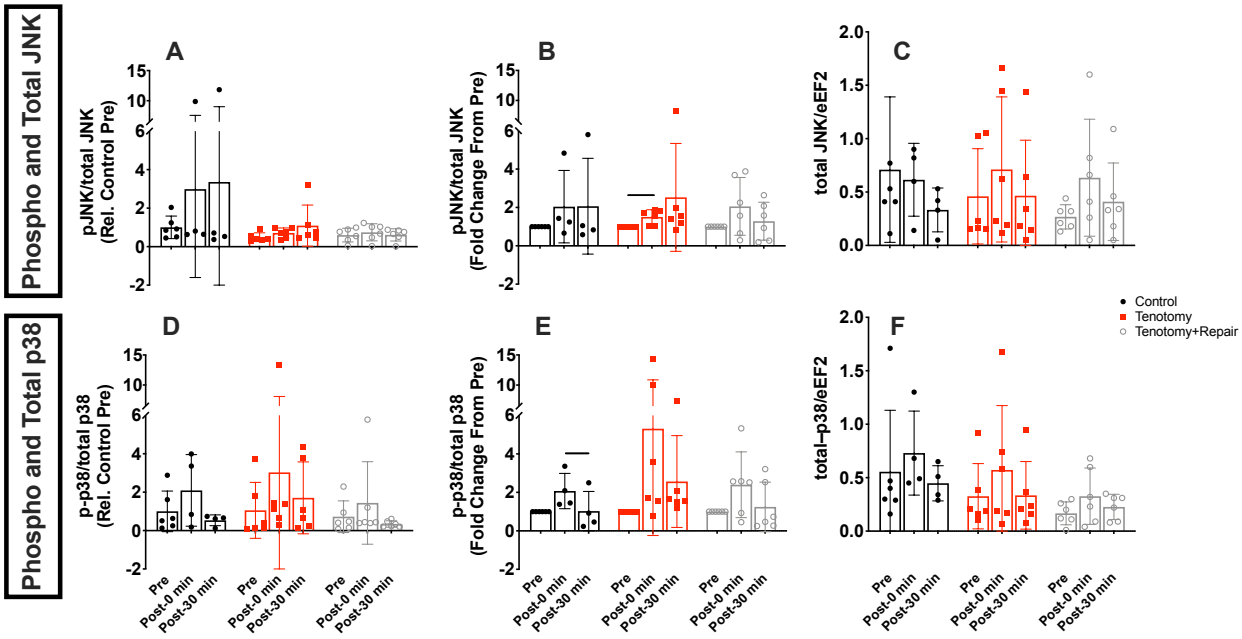

Figure 4.6. Immunoblotting results for total JNK, pJNK, total p38, and p-p38 for all groups (N=16; n=4 control, n=6 tenotomy, n=6 repair). Top row shows pJNK/totalJNK normalized to the mean of the control group's Pre (A), normalized to each animal's Pre biopsy (B), and total JNK normalized to eEF2 (C). Bottom row shows p-p38/total p38 normalized to the mean of the control group's Pre (D), normalized to each animal's Pre biopsy (E), and total p38 normalized to eEF2 (F). Bars are mean ± SD. One-way ANOVA with *post*-hoc Tukey's test was used to compare each group's Pre levels to the Control Pre (A and D). Two-way ANOVAs and *post-hoc* Tukey's tests were used to compare the main effect of contraction, simple effects of group, and simple effects of contraction within groups. All significance was set at $p < 0.05$.

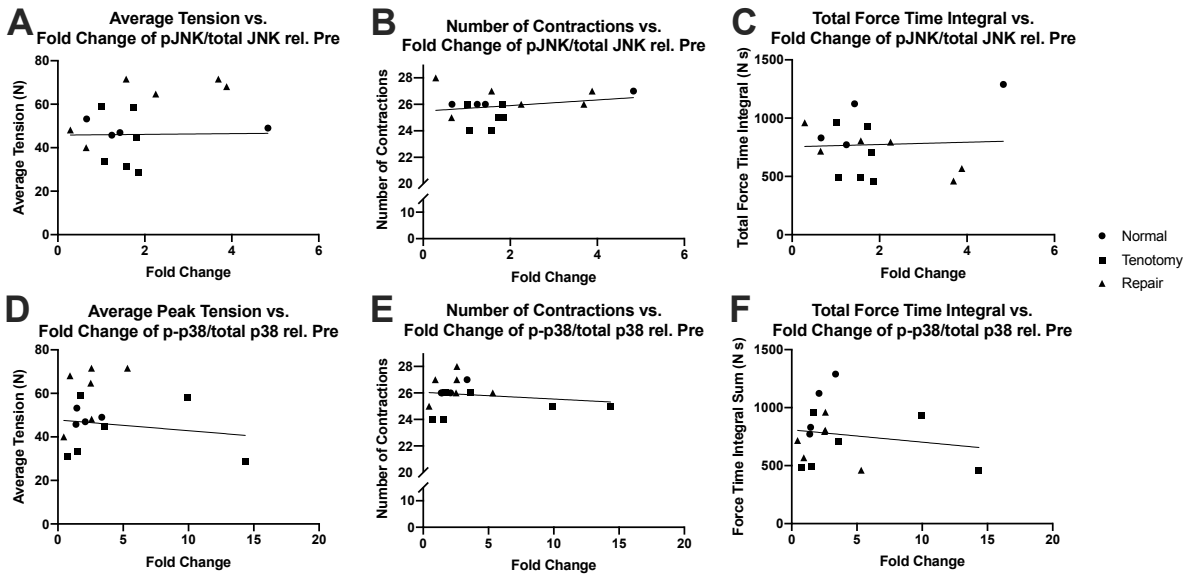

Figure 4.7. Linear regressions of fold change in phosphorylation/total JNK (top row) and p38 (bottom row) immediately after the exercise bout vs. average peak tension (A and D), number of contractions (B and E), and total force time integral (C and F). Regressions were pooled across all groups (N=16; n=4 control, n=6 tenotomy, n=6 repair).

References

1. Bamman MM, Roberts BM, Adams GR. Molecular Regulation of Exercise-Induced Muscle Fiber Hypertrophy. *Cold Spring Harb Perspect Med* 8: a029751, 2018. doi: 10.1101/cshperspect.a029751.

2. Boppart MD, Hirshman MF, Sakamoto K, Fielding RA, Goodyear LJ. Static stretch increases c-Jun NH2-terminal kinase activity and p38 phosphorylation in rat skeletal muscle. *Am J Physiol Cell Physiol* 280: C352-358, 2001. doi: 10.1152/ajpcell.2001.280.2.C352.

3. Choo A, McCarthy M, Pichika R, Sato EJ, Lieber RL, Schenk S, Lane JG, Ward SR. Muscle Gene Expression Patterns in Human Rotator Cuff Pathology. *J Bone Joint Surg Am* 96: 1558–1565, 2014. doi: 10.2106/JBJS.M.01585.

4. Close RI. Dynamic properties of mammalian skeletal muscles. *Physiol Rev* 52: 129–197, 1972. doi: 10.1152/physrev.1972.52.1.129.

5. Collin P, Colmar M, Thomazeau H, Mansat P, Boileau P, Valenti P, Saffarini M, Nover L, Kempf JF. Clinical and MRI Outcomes 10 Years After Repair of Massive Posterosuperior Rotator Cuff Tears. *The Journal of bone and joint surgery American volume* 100: 1854–1863, 2018. doi: 10.2106/JBJS.17.01190.

6. Fiatarone MA, Marks EC, Ryan ND, Meredith CN, Lipsitz LA, Evans WJ. High-Intensity Strength Training in Nonagenarians: Effects on Skeletal Muscle. *JAMA* 263: 3029–3034, 1990. doi: 10.1001/jama.1990.03440220053029.

7. Frey E, Regenfelder F, Sussmann P, Zumstein M, Gerber C, Born W, Fuchs B. Adipogenic and myogenic gene expression in rotator cuff muscle of the sheep after tendon tear. *Journal of Orthopaedic Research* 27: 504–509, 2009. doi: 10.1002/jor.20695.

8. Fujii N, Boppart MD, Dufresne SD, Crowley PF, Jozsi AC, Sakamoto K, Yu H, Aschenbach WG, Kim S, Miyazaki H, Rui L, White MF, Hirshman MF, Goodyear LJ. Overexpression or ablation of JNK in skeletal muscle has no effect on glycogen synthase activity. *American Journal of Physiology-Cell Physiology* 287: C200–C208, 2004. doi: 10.1152/ajpcell.00415.2003.

9. Gerber C, Schneeberger AG, Hoppeler H, Meyer DC. Correlation of atrophy and fatty infiltration on strength and integrity of rotator cuff repairs: a study in thirteen patients. *J Shoulder Elbow Surg* 16: 691–696, 2007. doi: 10.1016/j.jse.2007.02.122.

10. Gibbons MC, Fisch KM, Pichika R, Cheng T, Engler AJ, Schenk S, Lane JG, Singh A, Ward SR. Heterogeneous muscle gene expression patterns in patients with massive rotator cuff tears. *PLoS One* 13: e0190439, 2018. doi: 10.1371/journal.pone.0190439.

11. Gibbons MC, Singh A, Engler AJ, Ward SR. The role of mechanobiology in progression of rotator cuff muscle atrophy and degeneration. *J Orthop Res* 36: 546–556, 2018. doi: 10.1002/jor.23662.

12. Gladstone JN, Bishop JY, Lo IKY, Flatow EL. Fatty infiltration and atrophy of the rotator cuff do not improve after rotator cuff repair and correlate with poor functional outcome. *Am J Sports Med* 35: 719–728, 2007. doi: 10.1177/0363546506297539.

13. Glass DJ. Skeletal muscle hypertrophy and atrophy signaling pathways. *The International Journal of Biochemistry & Cell Biology* 37: 1974–1984, 2005. doi: 10.1016/j.biocel.2005.04.018.

14. Goutallier D, Postel JM, Bernageau J, Lavau L, Voisin MC. Fatty muscle degeneration in cuff ruptures. Pre- and postoperative evaluation by CT scan. *Clin Orthop Relat Res* : 78–83, 1994.

15. Goutallier D, Postel J-M, Gleyze P, Leguilloux P, Van Driessche S. Influence of cuff muscle fatty degeneration on anatomic and functional outcomes after simple suture of full-thickness tears. *J Shoulder Elbow Surg* 12: 550–554, 2003. doi: 10.1016/s1058-2746(03)00211-8.

16. Gumucio JP, Davis ME, Bradley JR, Stafford PL, Schiffman CJ, Lynch EB, Claflin DR, Bedi A, Mendias CL. Rotator cuff tear reduces muscle fiber specific force production and induces macrophage accumulation and autophagy. *J Orthop Res* 30: 1963–1970, 2012. doi: 10.1002/jor.22168.

17. Gumucio JP, Sugg KB, Mendias CL. TGF-β superfamily signaling in muscle and tendon adaptation to resistance exercise. *Exerc Sport Sci Rev* 43: 93–99, 2015. doi: 10.1249/JES.0000000000000041.

18. Hoppeler H, Klossner S, Flück M. Gene expression in working skeletal muscle. *Adv Exp Med Biol* 618: 245–254, 2007. doi: 10.1007/978-0-387-75434-5_19.

19. Hyman SA, Norman MB, Dorn SN, Bremner SN, Esparza MC, Lieber RL, Ward SR. In Vivo Supraspinatus Muscle Contractility and Architecture in Rabbit. .

20. Keener JD, Galatz LM, Stobbs-Cucchi G, Patton R, Yamaguchi K. Rehabilitation following arthroscopic rotator cuff repair: a prospective randomized trial of immobilization compared with early motion. *The Journal of bone and joint surgery American volume* 96: 11–9, 2014. doi: 10.2106/jbjs.m.00034.

21. Kramer HF, Goodyear LJ. Exercise, MAPK, and NF-κB signaling in skeletal muscle. *J Appl Physiol* 103: 8, 2007.

22. Lessard SJ, MacDonald TL, Pathak P, Han MS, Coffey VG, Edge J, Rivas DA, Hirshman MF, Davis RJ, Goodyear LJ. JNK regulates muscle remodeling via myostatin/SMAD inhibition. *Nature Communications* 9: 3030, 2018. doi: 10.1038/s41467-018-05439-3.

23. Liu X, Joshi SK, Samagh SP, Dang Y-X, Laron D, Lovett DH, Bodine SC, Kim HT, Feeley BT. Evaluation of Akt/mTOR activity in muscle atrophy after rotator cuff tears in a rat model. *J Orthop Res* 30: 1440–1446, 2012. doi: 10.1002/jor.22096.

24. Martineau LC, Gardiner PF. Insight into skeletal muscle mechanotransduction: MAPK activation is quantitatively related to tension. *J Appl Physiol (1985)* 91: 693–702, 2001. doi: 10.1152/jappl.2001.91.2.693.

25. McCracken TO, Kainer RA, Carlson D. Color Atlas of Small Animal Anatomy: The Essentials, Revised Edition [Online]. Wiley-Blackwell. https://www.wiley.com/en-us/Color+Atlas+of+Small+Animal+Anatomy%3A+The+Essentials%2C+Revised+Edition-p-9780813816081 [24 Aug. 2020].

26. Powell PL, Roy RR, Kanim P, Bello MA, Edgerton VR. Predictability of skeletal muscle tension from architectural determinations in guinea pig hindlimbs. *J Appl Physiol Respir Environ Exerc Physiol* 57: 1715–1721, 1984. doi: 10.1152/jappl.1984.57.6.1715.

27. Ruoss S, Möhl CB, Benn MC, von Rechenberg B, Wieser K, Meyer DC, Gerber C, Flück M. Costamere protein expression and tissue composition of rotator cuff muscle after tendon release in sheep. *J Orthop Res* 36: 272–281, 2018. doi: 10.1002/jor.23624.

28. Sandri M. Signaling in Muscle Atrophy and Hypertrophy. *Physiology* 23: 160–170, 2008. doi: 10.1152/physiol.00041.2007.

29. Shen P-H, Lien S-B, Shen H-C, Lee C-H, Wu S-S, Lin L-C. Long-term functional outcomes after repair of rotator cuff tears correlated with atrophy of the supraspinatus muscles on magnetic resonance images. *J Shoulder Elbow Surg* 17: 1S-7S, 2008. doi: 10.1016/j.jse.2007.04.014.

30. Somwar R, Perreault M, Kapur S, Taha C, Sweeney G, Ramlal T, Kim DY, Keen J, Côté CH, Klip A, Marette A. Activation of p38 Mitogen-Activated Protein Kinase ⎵ and ␋ by Insulin and Contraction in Rat Skeletal Muscle. 49: 7, 2000.

31. Thigpen CA, Shaffer MA, Gaunt BW, Leggin BG, Williams GR, Wilcox RB. The American Society of Shoulder and Elbow Therapists' consensus statement on rehabilitation following arthroscopic rotator cuff repair. *Journal of Shoulder and Elbow Surgery* 25: 521–535, 2016. doi: 10.1016/j.jse.2015.12.018.

32. Wang F, Murrell GAC, Wang M-X. Oxidative stress-induced c-Jun N-terminal kinase (JNK) activation in tendon cells upregulates MMP1 mRNA and protein expression. *Journal of Orthopaedic Research* 25: 378–389, 2007. doi: https://doi.org/10.1002/jor.20294.

33. Wilde JM, Gumucio JP, Grekin JA, Sarver DC, Noah AC, Ruehlmann DG, Davis ME, Bedi A, Mendias CL. Inhibition of p38 MAPK Signaling Reduces Fibrosis and Lipid Accumulation After Rotator Cuff Repair. *J Shoulder Elbow Surg* 25: 1501–1508, 2016. doi: 10.1016/j.jse.2016.01.035.

Chapter 5. Discussion

The purpose of Aim 1 was to determine the maximum contractile force and stress and, secondarily to understand the normal length-tension behavior for the rabbit SSP. We predicted the peak isometric tension using methods and architecture previously described (7, 12) to benchmark our experimental expectations. We measured maximum isometric force, which was significantly higher than previously described (2, 11). After performing a detailed architectural assessment of the SSP, we generated a theoretical length-tension curve to attempt to explain our experimental data based on classic muscle physiology (1). Using intact resting muscle length values and whole muscle contraction strain, we determined the *in vivo* operating range of the SSP. The activated muscle length-tension curve was computed by scaling resting muscle length by the strain decrease measured during contraction and is shifted left compared to the resting muscle length-tension curve, as it incorporates muscle shortening with tendon elongation during contraction.

The purpose of Aim 2 was to determine the structural and physiological consequences of rotator cuff tear and surgical repair over time through measuring muscle architecture and the length-tension relationship. Our hypotheses that architectural changes would demonstrate radial and longitudinal atrophy after tear and persist through repair, and that peak force would be decreased after tenotomy and repair, were supported. Muscle strain was lower after 8 wk tenotomy and repair, and similar to normal at 16 wk tenotomy and repair, refuting our hypothesis. Our hypothesis that length-tension curves would be narrower after tenotomy and repair was supported only after 16 wk repair, and it seemed that the length-tension curves varied for each intervention group in different ways. The architectural consequences of tenotomy indicate that muscle retraction and prolonged mechanical unloading lead to serial sarcomere loss, consistent with prior literature (3, 10). In summary, this study provided a detailed picture of the structural and physiological changes that occur in the rabbit SSP after tenotomy and repair over time.

The objective of Aim 3 was to determine if chronic tenotomy and/or repair influences the SSP's cell signaling response to a contractile stimulus. Our hypothesis that there would be lower phosphorylation of JNK and p38 in the tenotomized and repaired muscles compared to control muscles was refuted, as there was a similar fold change increase in phosphorylation after contraction regardless of group. Despite the 33% lower peak force production for tenotomy and 25% reduced force production for repair, peak muscle stresses are not significantly different. Similarly, there was a 25% reduction in average tension and 33% reduction in force-time integral after tenotomy, that did not improve after repair. Since the muscles in the tenotomy and repair groups are achieving similar muscle stresses as the control rabbits, the effective "duty cycle" for each group is roughly the same, as the atrophied muscles in tenotomy and repair are able to achieve normal stress levels even though their overall force output is lower. We found increased phosphorylation of JNK and p38 across groups, but there were no significant differences in basal levels of pJNK or p38, and no significant differences in total JNK or p38 between groups. Taken together, this indicates that the muscles are still behaving relatively normal in terms of MAPK mechanotransduction (1, 8)

While we were able to reach important conclusions in this work, there are also several limitations. First, the rabbit model of rotator cuff tear and repair offers many benefits in a lab setting, but is not able to fully recapitulate the severe clinical phenotype observed in humans (4). Chronic RC tears in humans develop over multiple years, as opposed to our acute rabbit injury model which develops for 8 or 16 weeks. As a result, we see large degrees of fatty infiltration close to the myotendinous junction, but less throughout the medial aspects of the muscle (unpublished data). Second, the "exercise" experiment performed here would be impossible in a clinical setting, as maximal intensity contractions via direct nerve stimulation have several differences over volitional activation by a patient. Similarly, the protocol we employed is an order of magnitude less severe than what is used in rats, so the magnitude of signaling response we could achieve was lower than previously reported (6). However, this contraction protocol

was more clinically relevant, as recovering RC tear patients likely are unable to rapidly perform several hundred contractions (5, 9)

In summary, this dissertation provided a detailed method to measure whole muscle physiology, and extensive structural and physiological analysis of rabbit RC muscles in healthy and pathological states. Active length-tension curves were predicted using a relatively simple model for the rabbit supraspinatus (SSP). Under normal conditions, active function relied heavily on architectural parameters. However, after chronic tenotomy and surgical repair, architectural parameters alone could predict peak muscle force, but are not sufficient to predict other physiological characteristics in the muscle. Activation of MAPKs after an exercise bout, which are known to be mechanosensing, were not decreased after tenotomy or repair, indicating relatively normal muscle activation in response to mechanical stress. Overall, this work sheds new light onto the physiological consequences of chronic rotator cuff tear and repair, offering new methods to test potential therapies and opening new avenues for understanding their clinical impact based on functional metrics.

References

1. Close RI. Dynamic properties of mammalian skeletal muscles. *Physiol Rev* 52: 129–197, 1972. doi: 10.1152/physrev.1972.52.1.129.

2. Fabis J, Kordek P, Bogucki A, Mazanowska-Gajdowicz J. Function of the rabbit supraspinatus muscle after large detachment of its tendon: 6-week, 3-month, and 6-month observation. *Journal of Shoulder and Elbow Surgery* 9: 211–6, 2000.

3. Gibbons MC, Singh A, Anakwenze O, Cheng T, Pomerantz M, Schenk S, Engler AJ, Ward SR. Histological Evidence of Muscle Degeneration in Advanced Human Rotator Cuff Disease. *The Journal of bone and joint surgery American volume* 99: 190–199, 2017. doi: 10.2106/jbjs.16.00335.

4. Goutallier D, Postel JM, Bernageau J, Lavau L, Voisin MC. Fatty muscle degeneration in cuff ruptures. Pre- and postoperative evaluation by CT scan. *Clin Orthop Relat Res* : 78–83, 1994.

5. Keener JD, Galatz LM, Stobbs-Cucchi G, Patton R, Yamaguchi K. Rehabilitation following arthroscopic rotator cuff repair: a prospective randomized trial of immobilization compared with early motion. *The Journal of bone and joint surgery American volume* 96: 11–9, 2014. doi: 10.2106/jbjs.m.00034.

6. Martineau LC, Gardiner PF. Insight into skeletal muscle mechanotransduction: MAPK activation is quantitatively related to tension. *J Appl Physiol (1985)* 91: 693–702, 2001. doi: 10.1152/jappl.2001.91.2.693.

7. Mathewson MA, Kwan A, Eng CM, Lieber RL, Ward SR. Comparison of rotator cuff muscle architecture between humans and other selected vertebrate species. *J Exp Biol* 217: 261–273, 2014. doi: 10.1242/jeb.083923.

8. Powell PL, Roy RR, Kanim P, Bello MA, Edgerton VR. Predictability of skeletal muscle tension from architectural determinations in guinea pig hindlimbs. *J Appl Physiol Respir Environ Exerc Physiol* 57: 1715–1721, 1984. doi: 10.1152/jappl.1984.57.6.1715.

9. Thigpen CA, Shaffer MA, Gaunt BW, Leggin BG, Williams GR, Wilcox RB. The American Society of Shoulder and Elbow Therapists' consensus statement on rehabilitation following arthroscopic rotator cuff repair. *Journal of Shoulder and Elbow Surgery* 25: 521–535, 2016. doi: 10.1016/j.jse.2015.12.018.

10. Tomioka T, Minagawa H, Kijima H, Yamamoto N, Abe H, Maesani M, Kikuchi K, Abe H, Shimada Y, Itoi E. Sarcomere length of torn rotator cuff muscle. *Journal of Shoulder and Elbow Surgery* 18: 955–9, 2009. doi: 10.1016/j.jse.2009.03.009.

11. Valencia AP, Iyer SR, Pratt SJP, Gilotra MN, Lovering RM. A method to test contractility of the supraspinatus muscle in mouse, rat, and rabbit. *J Appl Physiol (1985)* 120: 310–7, 2016. doi: 10.1152/japplphysiol.00788.2015.

12. Winters TM, Takahashi M, Lieber RL, Ward SR. Whole muscle length-tension relationships are accurately modeled as scaled sarcomeres in rabbit hindlimb muscles. *Journal of Biomechanics* 44: 109–115, 2011. doi: 10.1016/j.jbiomech.2010.08.033.